Journal of Intelligent & Robotic Systems (2024) 110:63
https://doi.org/10.1007/s10846-024-02088-1

REGULAR PAPER

Adaptive Non-singular Fast Terminal Sliding Mode Control for Car-Like Vehicles with Faded Neighborhood Information and Actuator Faults

Mahmoud Hussein[1] · Youmin Zhang[2] · Zhaoheng Liu[3]

Received: 20 May 2023 / Accepted: 4 March 2024

Abstract

This study addresses the problem of cooperative control design for a group of car-like vehicles encountering fading channels, actuator faults, and external disturbances. It is presumed that certain followers lack direct access to the states of the leader via a directed graph. This arises challenges in maintaining synchronization and coordination within the network. The proposed control strategy utilizes non-singular fast terminal sliding mode control to accelerate consensus tracking and enhance the convergence of the overall system. This controller is designed to mitigate the impact of actuator faults in the presence of fading channels in the communication network. The effects of such issues on team performance are rigorously analyzed. Based on the Lyapunov stability principle, it has been demonstrated that the controller is capable of providing satisfactory performance for the entire system despite these challenges. Moreover, vehicle synchronization can be effectively maintained. Numerical simulations are conducted to verify the theoretical findings.

Keywords Car-like vehicle · Faded neighborhood information channel · Fault-tolerant control · Actuator faults · Non-singular fast terminal sliding mode · Adaptive control

1 Introduction

Recent years have witnessed an increasing interest in the control community to study the challenges associated with the development of cooperative controls for Networked Control Systems (NCSs). These challenges involve the coordination of various tasks, including but not limited to spacecrafts, unmanned aerial vehicles, and mobile robots [1, 2]. Cooperative control primarily focuses on the consensus problem, this entails developing an algorithm that ensures all vehicles in the system reach an agreement on a common goal or state. Numerous studies have been documented concerning consensus issues of first-order [3, 4], second-order [5, 6], and high-order systems [7]. Consensus problems were primarily investigated within the linear systems [8].

Studying consensus in nonlinear systems poses greater challenges compared to linear systems. However, nonlinearity is pervasive in practice, and several studies have been carried out to investigate nonlinear dynamic systems [9, 10]. For instance, the authors in [11] introduced a control methodology for nonlinear systems utilizing a backstepping approach to mitigate the effects of hysteretic actuator faults. However, it is worth mentioning that the unknown components of the nonlinear systems were assumed to have linear parameters. In other related studies, the effects of stochastic disturbances on systems with nonlinear behavior have been investigated in [12] and [13]. It is recognized that stability issues in such systems present a greater challenge to resolve compared to deterministic systems. A physical system is inherently nonlinear. It is therefore important to consider nonlinearity when studying NCSs. It is clear that consensus research for NCSs that considers non-linearity is of increasing significance [14]. As a means of handling the consensus problem associated with stochastic disturbances, two dif-

✉ Youmin Zhang
youmin.zhang@concordia.ca

Mahmoud Hussein
mahmoud.hussein.1@ens.etsmtl.ca

Zhaoheng Liu
zhaoheng.liu@etsmtl.ca

1 Department of Electrical Engineering, École de technologie supérieure, QC H3C 1K3 Montréal, Canada

2 Department of Mechanical, Industrial, and Aerospace Engineering, Concordia University, QC H3G 1M8 Montréal, Canada

3 Department of Mechanical Engineering, École de technologie supérieure, QC H3C 1K3 Montréal, Canada

Published online: 18 April 2024

ferent delay-free impulsive pinning control methods were proposed in [15]. The proposed methods, however, cannot ensure synchronization among team members. Sliding Mode Control (SMC) is a reliable strategy for handling uncertainties and external disturbances in nonlinear systems. In [14], for instance, tracking of consensus in finite time for NCSs under uncertainty and perturbation is effectively attained by employing the SMC technique alongside a time-varying approach capable of accommodating temporal fluctuations and uncertainties.

In practical applications, convergence emerges as a crucial metric for assessing the tracking error mechanism. Convergence over finite-time consensus can be achieved at a faster rate than asymptotic convergence. Hence, it is imperative to conduct further investigations into NCSs within the framework of finite-time consensus. While the Terminal Sliding Mode Control (TSMC) method is highly responsive, resilient, and offers a high degree of convergence in a finite time, it may however encounter singularity problems as errors approach zero, potentially resulting in unbounded parameters. The Non-singular Terminal Sliding Mode Control (NTSMC) approach has been developed to mitigate this limitation [16]. Further, an improved form of NTSMC, known as the Non-singular Fast Terminal Sliding Mode Control (NFTSMC) has been developed by some researchers. The NFTSMC offers a faster convergence to the state variables compared to the NTSMC, preserving the advantages of the NTSMC [17, 18]. However, various practical challenges persist, including communication network faults, state limitations, and actuator faults, among others, which remain difficult to address while ensuring the necessary system performance. It is known that actuator failure is a common fault encountered in physical systems, which can cause instability in individual subsystems, ultimately failing the overall system [19]. None of the studies mentioned earlier addressed the problem of component faults as well as their influence on the stability of networked systems. Hence, this study is motivated by a need to fill this gap in the literature.

Actuator faults can manifest in physical systems due to various reasons such as component aging, power issues, or uncontrolled crashing. Previous studies [20–22] examined faults of actuators, including those that result in loss of effectiveness and bias. Aside from commonly used approaches like Linear Matrix Inequality (LMI) approaches [23], and Fault Detection and Isolation (FDI)-based methods [24, 25], an adaptive approach has been recognized as an efficient method for mitigating various types of actuator faults [26, 27]. Nevertheless, the proposed methodologies would be impractical if agents cannot share complete state information due to issues such as fading channels, time delays, or packet losses.

In light of the extensive integration of wireless communication technologies into practical systems, we address a prevalent issue known as fading channels. Fading is one of the most significant phenomena that occurs in wireless networks as a result of diffraction, reflection, and refraction during propagation [28]. Essentially, fading occurs due to the reduction in signal strength as transmitted data travels through particular propagation mediums. This leads to a deterioration in the shared state information among agents, encompassing parameters such as displacement, speed, and others that are crucial for the development of controllers and maintenance of systems' stability [29]. Several studies have examined the stability of NCSs in the presence of fading channels [30, 31]. In [30], the authors employed a learning algorithm to enhance linear system tracking performance in the presence of faded information, all without enforcing stringent restrictions on the characteristics of the fading channel. An optimization framework based on Kalman filtering is used in [32] for optimizing the learning gain by incorporating the covariance matrix of the input error. In [31], a control scheme that relies on approximation is utilized to address the tracking problem for systems with unknown dynamics and fading channels. The proposed framework models random signals as a combination of multiplicative and additive stochastic components. There are further studies related to this issue in [33, 34]. Until now, the control tracking issue for NCSs facing challenges commonly encountered on large-scale systems such as actuator faults, fading channels, and external disturbances has not been studied.

Numerous studies have recently examined the stability of NCSs with actuator faults, including those discussed in [25, 35, 36]. The authors in [25] proposed a fractional-order sliding-mode control strategy for a team of Unmanned Aerial Vehicles (UAVs) subject to actuator faults during a fire monitoring mission. The actuator faults and the external disturbances are estimated by sliding-mode disturbance observers. In [35], an event-triggered adaptive fault-tolerant control method was developed for a class of nonlinear multi-agent systems with actuator and sensor faults. The control design incorporates fault compensation mechanism and command filtering methods to avoid duplicative differentiation leading to a burst of complexity. The study in [36] investigated the fault-tolerant tracking problem of time-varying formation for nonholonomic multi-robot systems. Fuzzy logic systems are used to approximate uncertain nonlinear dynamics, and an adaptive backstepping recursive procedure and dynamic surface technology are used to develop a fuzzy adaptive formation tracking control scheme. Furthermore, a decentralized adaptive fault-tolerant control strategy was proposed to compensate for actuator faults and ensure that all signals are semi-globally uniformly and ultimately bounded.

However, the above-mentioned studies have the limitations of assuming that the state information exchanged between vehicles is always available and that there is no faded neighborhood information in the network. It is challenging to develop a fault-tolerant cooperative control algorithm for NCSs when considering the actuator faults problem with the lack of complete state information shared in the network. The purpose of a fault-tolerant controller is to cope with the faults of actuators and achieve a certain group behavior with acceptable performance. Nevertheless, this objective cannot be accomplished when the vehicles share their state information via fading channels.

In the fading channels condition, if one vehicle's actuator fails, its impact can spread to other vehicles, severely degrading the overall system performance. This limitation motivated us to address the actuators' and fading channels' issues and investigate how they impact the stability of networked systems. In contrast to the control methods proposed in the relative studies, our developed controller can handle actuator faults in the presence of faded state information. Moreover, it is more responsive, robust, and stable in unknown circumstances. To the authors' best knowledge, this is the first attempt to address such a challenging problem for a team of car-like vehicles.

Inspired by the preceding discussions, this paper investigates the problem of cooperative control design for NCSs affected by fading channels, actuator faults, and external disturbances. To this end, we develop an Adaptive Nonsingular Fast Terminal Sliding Mode Control (ANFTSMC) for a group of car-like vehicles. This controller enables each vehicle to mitigate the effects of faults, if present, and complete the mission with the other members of the team. Our first step involves establishing an ANFTSMC mechanism to address the challenges posed by fading channels and external disturbances. Then, we develop an ANFTSMC strategy considering the effects of actuator faults, fading channels, and external disturbances. The developed methodologies have the capability of overcoming the singularity and providing fast convergence of the team members to reach a consensus.

The contributions of this research can be outlined as follows:

1. Different from [25] and [35–37], our study introduces a feasible methodology to handle the actuator faults of vehicles interacting over fading communication channels and subject to external disturbances.
2. This developed controller introduces an adaptive mechanism that allows for the automatic modification of the control gain, which differs from the sliding mode protocols described in [38] and [39]. This presents an advantage compared to a constant control gain, as sliding mode control can operate effectively with no prior knowledge of disturbances and uncertainties within the system.
3. In comparison with existing methods of fault-tolerant control design, the proposed ANFTSMC features a simple structure and can be easily implemented in various applications.

The subsequent sections of this paper are structured as follows: Section 2 introduces preliminaries and problem formulation. In Section 3, a controller is proposed for leader-follower systems impacted by fading channels, actuator faults, and external disturbances. Section 4 includes numerical simulations to validate the effectiveness of the proposed approach. Finally, Section 5 presents a conclusion and outlines potential avenues for future research.

2 Preliminaries and Problem Formulation

2.1 Graph theory [40]

The graph $\boldsymbol{G} = (\boldsymbol{V}, \boldsymbol{E}, \boldsymbol{A})$ depicts the communication topology of a team, with $\boldsymbol{V} = \{v_1, v_2, ..., v_n\}$ representing the vertex set and $\boldsymbol{E} = \{e_{ij} = (v_i, v_j)\}$ denoting the set of edges. An adjacency matrix $\boldsymbol{A}$ is defined as $\boldsymbol{A} = [a_{ij}]_{n\times n}$, where $a_{ij} > 0$ signifies the existence of an edge between node v_i and node v_j, and $a_{ij} = 0$ indicates the absence of such an edge. A graph G is considered strongly connected if there is a path connecting every pair of distinct nodes v_i and v_j.

A weighted graph's Laplacian matrix is defined as follows:

$$\boldsymbol{L_m} = \boldsymbol{D} - \boldsymbol{A} = [l_{ij}] \in \mathbb{R}^{n\times n} \tag{1}$$

In this context, the degree matrix $\boldsymbol{D} = \mathrm{diag}(d_1, d_2, ...d_n)$, where $d_i = \sum_{j=1}^{N} a_{ij}$, $l_{ij} = -a_{ij}$, $\forall j \neq i$ and $\sum_{j=1}^{N} l_{ij} = l_{ii}$, $\forall i = 1, 2, ..., N$.

This research examines a group of vehicles with l representing the leader and $i = 1, 2, ..., N$ denoting the followers. Digraphs G are employed to illustrate the communication among leaders and followers. The diagonal matrix $\boldsymbol{B} = \mathrm{diag}(b_1, b_2, ..., b_N)$ captures the direct communication between the leader and followers, where $b_i = 1$ signifies direct communication, and zero otherwise.

2.2 System description

In this study, it is assumed that the system comprises one virtual leader and multiple followers. The dynamics pertaining to i^{th} $(i = 1, 2, ..., N)$ follower can be described as follows:

$$\begin{cases} \dot{\boldsymbol{q}}_i &= \boldsymbol{J}_i \bar{\boldsymbol{\omega}}_i \\ \dot{\bar{\boldsymbol{\omega}}}_i &= \bar{\boldsymbol{M}}^{-1} \bar{\boldsymbol{B}}(\boldsymbol{q}_i)\boldsymbol{\tau}_i - \boldsymbol{h}_i(\boldsymbol{q}_i, \bar{\boldsymbol{\omega}}_i) + \boldsymbol{d}_i \end{cases} \tag{2}$$

Similarly, the dynamics of a leader can be presented as follows:

$$\begin{cases} \dot{\boldsymbol{q}}_l &= \boldsymbol{J}_i \bar{\boldsymbol{\omega}}_l \\ \dot{\bar{\boldsymbol{\omega}}}_l &= \bar{\boldsymbol{M}}^{-1} \bar{\boldsymbol{B}}(\boldsymbol{q}_l)\boldsymbol{\tau}_l - \boldsymbol{h}_l(\boldsymbol{q}_l, \bar{\boldsymbol{\omega}}_l) \end{cases} \tag{3}$$

where

$$\boldsymbol{h}_i(\boldsymbol{q}_i, \bar{\boldsymbol{\omega}}_i) = \bar{\boldsymbol{M}}^{-1}\bar{\boldsymbol{V}}(\boldsymbol{q}_i, \dot{\boldsymbol{q}}_i)\bar{\boldsymbol{\omega}}_i; \quad \boldsymbol{h}_l(\boldsymbol{q}_l, \bar{\boldsymbol{\omega}}_l) = \bar{\boldsymbol{M}}^{-1}\bar{\boldsymbol{V}}(\boldsymbol{q}_l, \dot{\boldsymbol{q}}_l)\bar{\boldsymbol{\omega}}_l$$

$$\bar{\boldsymbol{\omega}}_i = \begin{bmatrix} v_i & w_i \end{bmatrix}^T; \quad \bar{\boldsymbol{M}} = \boldsymbol{J}_i^T \boldsymbol{M} \boldsymbol{J}_i; \quad \bar{\boldsymbol{V}} = \boldsymbol{J}_i^T(\boldsymbol{M}\dot{\boldsymbol{J}}_i + \boldsymbol{V}\boldsymbol{J}_i)$$

$$\bar{\boldsymbol{B}} = \boldsymbol{J}_i^T \boldsymbol{\Gamma}; \quad \boldsymbol{J}_i = \begin{bmatrix} \cos\phi_i & 0 \\ \sin\phi_i & 0 \\ \frac{tan(\psi_i)}{L} & 0 \\ 0 & 1 \end{bmatrix}$$

$$\boldsymbol{M} = \begin{bmatrix} m & 0 & I_c\sin(\phi_i) & 0 \\ 0 & m & -I_c\cos(\phi_i) & 0 \\ I_c\sin(\phi_i) & -I_c\cos(\phi_i) & I_b & I_w \\ 0 & 0 & I_w & I_w \end{bmatrix}$$

$$\boldsymbol{V} = \begin{bmatrix} 0 & 0 & -I_c\dot{\phi}\cos(\phi_i) & 0 \\ 0 & 0 & -I_c\dot{\phi}\sin(\phi_i) & 0 \\ 0 & 0 & 0 & 0 \\ 0 & 0 & 0 & 0 \end{bmatrix}; \quad \boldsymbol{\Gamma} = \begin{bmatrix} \cos(\phi_i) & 0 \\ \sin(\phi_i) & 0 \\ L\sin(\psi_i)\cos(\psi_i) & 0 \\ 0 & 1 \end{bmatrix}$$

where $\boldsymbol{q}_l = (x_l, y_l, \phi_l, \psi_l)^T$ and $\boldsymbol{q}_i = (x_i, y_i, \phi_i, \psi_i)^T$ denote the state vectors of the leader and i^{th} follower respectively. As shown in Fig. 1, the coordinates (x_i, y_i) represent the position of i^{th} follower. The state variables v_i and ω_i, denote the linear and steering velocities respectively. The variables ψ_i and ϕ_i represent the steering and heading angles of i^{th} follower. The torque applied to the actuators of the i^{th} follower is denoted by τ_i. The external disturbances acting on the system are represented by $\boldsymbol{d}_i$.

The equations provided represent the following parameters: $m = m_c + 4m_w$ represents the total mass, where m_c denotes the vehicle mass and m_w deontes the mass of each wheel. $I_c = (L-b)m_c + 2Lm_w$ represents the inertia about the center of mass, where L denotes the length between the vehicle's axles and b represents the length from the front axle to the mass center. $I_b = m_c(L-b)^2 + 4W^2 m_w + I_{bzz} + 4I_{wzz}$, refers to the inertia about the mass center of the entire vehicle, where W denotes the width of the vehicle and I_w and I_{bzz} represent the inertia about the vertical axis for the vehicle and each wheel respectively. As illustrated in Fig. 1, CoR (Center of Rotation) is a center of rotation around the rear wheel axis.

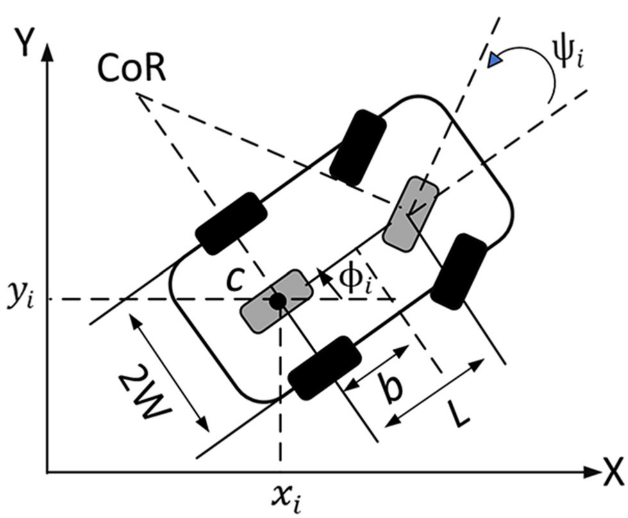

Fig. 1 Car-like vehicle reference frame and parameters

Assumption 1 *There exists a positive constant $\bar{d}$ such that $||d_i|| < \bar{d}$, representing an upper bound for the external disturbances.*

Assumption 2 [41] *For any $\boldsymbol{q}_i$, $\bar{\boldsymbol{\omega}}_i$,i $\in$ [1,...,N], there exist positive constants μ_1 and μ_2 so that:*

$$\|\boldsymbol{H}(\boldsymbol{q}, \bar{\boldsymbol{\omega}}, t) - \boldsymbol{1} \otimes \boldsymbol{h}(\boldsymbol{q}_l, \bar{\boldsymbol{\omega}}_l, t)\| \leq \mu_1\|\boldsymbol{q} - \boldsymbol{1} \otimes \boldsymbol{q}_l\| + \mu_2\|\bar{\boldsymbol{\omega}} - \boldsymbol{1} \otimes \bar{\boldsymbol{\omega}}_l\| \quad (4)$$

where $\boldsymbol{H}(\boldsymbol{q}, \bar{\boldsymbol{\omega}}, t) = [\boldsymbol{h}_1(\boldsymbol{q}_1, \bar{\boldsymbol{\omega}}_1), ..., \boldsymbol{h}_N(\boldsymbol{q}_N, \bar{\boldsymbol{\omega}}_N)]^T$, and $\otimes$ *is the Kronecker product.*

Remark 1 *Assumption 2 holds significant importance in the development of the control law, as it ensures that the solution is uniquely determined. This premise holds true when the function $h(q, \bar{\omega})$ exhibits continuity and boundedness. The utilization of the Lipschitz condition for the function h limits the variation rate of the function. Thus, ensuring function boundedness involves considering the Lipschitz condition. In practice, compliance with Assumption 2 enables the controller to achieve vehicle convergence towards the predefined reference trajectory.*

Lemma 1 *The invertibility of the matrix $(\boldsymbol{L_m} + \boldsymbol{B})$ is contingent upon the existence of a directed spanning tree within the digraph G.*

Definition 1 [42] *For any interconnected system, the tracking error is said to be cooperatively uniformly ultimately bounded if a compact set $\bar{\theta}^{\varepsilon_1} \subset \mathbb{R}^N$ and $\bar{\theta}^{\varepsilon_2} \subset \mathbb{R}^N$ exists with the property that $\{0\} \subset \bar{\theta}^{\varepsilon_1}$ and $\{0\} \subset \bar{\theta}^{\varepsilon_2}$, $\forall\ \varepsilon_1 \in \bar{\theta}^{\varepsilon_1}$ and $\varepsilon_2 \in \bar{\theta}^{\varepsilon_2}$ there exist bounds $\bar{B}^{\varepsilon_1}$ and $\bar{B}^{\varepsilon_2}$ and time $T(\bar{B}^{\varepsilon_1}, \bar{B}^{\varepsilon_2}, \varepsilon_1, \varepsilon_2)$ such that $\|\varepsilon_1\| \leq \bar{B}^{\varepsilon_1}$, $\|\varepsilon_2\| \leq \bar{B}^{\varepsilon_2}$, $\forall t \geq t_o + T_a$, where ε_1 and ε_2 are the position and velocity tracking errors of the system, respectively.*

Remark 2 *The primary objective of cooperative control systems employing the leader-follower approach is to direct the followers to track the leader's state information. However, achieving precise control tracking in practice is hindered by challenges such as unknown dynamics, external disturbances, and component faults. To address these issues, the Cooperative Uniform Ultimate Boundedness (CUUB) approach is introduced to manage unforeseen variations encountered in real-world scenarios.*

In fault-free scenarios, the tracking error variables for the i^{th} follower can be written as follows: [43]:

$$\begin{cases} \boldsymbol{e}_{1i} &= \sum_{j=1}^{N} a_{ij}(\boldsymbol{p}_i - \boldsymbol{p}_j - \boldsymbol{\Delta}_{ij}) + b_i(\boldsymbol{p}_i - \boldsymbol{p}_L - \boldsymbol{\Delta}_{iL}) \\ \boldsymbol{e}_{2i} &= \sum_{j=1}^{N} a_{ij}(\bar{\boldsymbol{\omega}}_i - \bar{\boldsymbol{\omega}}_j) + b_i(\bar{\boldsymbol{\omega}}_i - \bar{\boldsymbol{\omega}}_l) \end{cases} \tag{5}$$

where $\boldsymbol{e}_{1i}$ and $\boldsymbol{e}_{2i}$ represent the position and velocity tracking error variables respectively. $a_{ij} = 1$ whenever there is a communication between i^{th} follower and its neighbor j; if not, it is zero. $\boldsymbol{p}_i = (x_i, y_i, \psi_i)^T$ and $\boldsymbol{\Delta}_{ij} = (\boldsymbol{\Delta}_j - \boldsymbol{\Delta}_i)$ is the measure of the distance and orientation of the i^{th} follower with respect to its neighbor j. $\boldsymbol{\Delta}_{iL}$ is the measure of the displacement and orientation of the i^{th} follower with respect to the leader.

Remark 3 *The tracking error defined in (5) is formulated to fulfill the primary objective of cooperative system design. This system is developed to guide all followers to accurately trace their designated reference trajectories while maintaining prescribed relative distances, essential for accomplishing specific cooperative tasks. Moreover, followers are expected to synchronize their velocities with that of the leader. The desired relative distance, denoted by $\Delta_{ij} = (x_{ij}, y_{ij}, \phi_{ij})$, assumes a pivotal role in shaping the intended structure of the team formation to effectively execute cooperative tasks. Through the incorporation of Δ_{ij} into the system, the controller can effectively manipulate follower movements, ensuring the convergence of $\boldsymbol{e}_{1i}$ and $\boldsymbol{e}_{2i}$ towards zero, thereby achieving precise trajectory tracking.*

When the error variables in Eq. 5 approach zero, the followers achieve the consensus while tracking the leader's coordinates. To simplify notation, Eq. 5 can be expressed in a compact form as follows:

$$\begin{cases} \boldsymbol{\varepsilon}_1 &= (\boldsymbol{L_m} + \boldsymbol{B}) \otimes \boldsymbol{I_m}.\tilde{\boldsymbol{p}} \\ \boldsymbol{\varepsilon}_2 &= (\boldsymbol{L_m} + \boldsymbol{B}) \otimes \boldsymbol{I_m}.\tilde{\bar{\boldsymbol{\omega}}} \end{cases} \tag{6}$$

where $\boldsymbol{\varepsilon}_1 = [\boldsymbol{e}_{11}, \ldots, \boldsymbol{e}_{1N}]^T, \boldsymbol{\varepsilon}_2 = [\boldsymbol{e}_{21}, \ldots, \boldsymbol{e}_{2N}]^T, \tilde{\boldsymbol{p}} = \boldsymbol{p} - 1 \otimes (\boldsymbol{p}_l - \boldsymbol{\Delta}_{iL}), \tilde{\bar{\boldsymbol{\omega}}} = \tilde{\bar{\boldsymbol{\omega}}} - \mathbf{1} \otimes \tilde{\bar{\boldsymbol{\omega}}}_l, \boldsymbol{I_m} \in R^{m \times m}$.

The derivative of Eq. 6 can be written as:

$$\begin{cases} \dot{\boldsymbol{\varepsilon}}_1 &= \bar{\boldsymbol{\varepsilon}}^\star_2 \\ \dot{\boldsymbol{\varepsilon}}_2 &= (\boldsymbol{L_m} + \boldsymbol{B}) \otimes \boldsymbol{I_m} \Big(\boldsymbol{H} - \mathbf{1} \otimes \boldsymbol{h}(\boldsymbol{q}_l, \bar{\boldsymbol{\omega}}_l) + \bar{\boldsymbol{M}}^{-1} \boldsymbol{\tau} - \mathbf{1} \otimes \bar{\boldsymbol{M}}^{-1} \boldsymbol{\tau}_l \Big) \end{cases} \tag{7}$$

where

$$\bar{\boldsymbol{\varepsilon}}^\star{}_2 = \bar{\boldsymbol{J}} \boldsymbol{\varepsilon}_2; \quad \bar{\boldsymbol{J}} = [\bar{\boldsymbol{J}}_1, \bar{\boldsymbol{J}}_2, ..., \bar{\boldsymbol{J}}_N]^T; \quad \bar{\boldsymbol{J}}_i = \begin{bmatrix} \cos\phi_i 0 \\ \sin\phi_i & 0 \\ \frac{tan(\psi_i)}{L} & 0 \end{bmatrix};$$

$$\boldsymbol{\tau} = [\boldsymbol{\tau}_1, ..., \boldsymbol{\tau}_N]^T \quad \text{and} \quad \boldsymbol{M}^{-1} = \text{diag}[\boldsymbol{M}_1^{-1}, ..., \boldsymbol{M}_N^{-1}]^T.$$

The objective set forth in Eq. 7 is to attain $\lim_{t\to\infty} \varepsilon_1 = 0$ and $\lim_{t\to\infty} \varepsilon_2 = 0$. However, when faced with degraded neighborhood data and faults in actuators, reaching this goal becomes impracticable unless the effects of such faults are taken into account during system design. Therefore, it is imperative to incorporate the effects of such faults into the system design to effectively address these challenges.

2.3 Modeling of fading channels

In practical systems, many factors can obstruct the communication of information among agents, leading to agents receiving distorted information instead of the precise data sent by their neighbors. In this work, we propose the hypothesis that signal fading only takes place as part of the exchange of data between followers, without any fading influencing the transmission of state information between the followers and leader.

The fading channels can be described in the following manner:

$$\begin{cases} \boldsymbol{p}^\star_j &= \frac{\mathbf{1}}{\delta^\star} \boldsymbol{\delta}_{ij} \boldsymbol{p}_j \\ \bar{\boldsymbol{\omega}}^\star_j &= \frac{1}{\delta^\star} \boldsymbol{\delta}_{ij} \bar{\boldsymbol{\omega}}_j \end{cases} \tag{8}$$

where $\boldsymbol{\delta}_{ij}$ stands for the attenuation parameter, while $\delta^\star$ denotes the mean value. $\boldsymbol{p}^\star_j$ and $\bar{\boldsymbol{\omega}}^\star_j$ represent information pertaining to faded state that i^{th} follower is receiving from neighbor j. Thus, Eq. 5 can be rewritten as follows:

$$\begin{cases} \boldsymbol{e}^\star{}_{1i} &= \sum_{j=1}^{N} a_{ij}(\boldsymbol{p}_i - \boldsymbol{p}^\star_j - \boldsymbol{\Delta}_{ij}) + b_i(\boldsymbol{p}_i - \boldsymbol{p}_L - \boldsymbol{\Delta}_{iL}) \\ \boldsymbol{e}^\star_{2i} &= \sum_{j=1}^{N} a_{ij}(\bar{\boldsymbol{\omega}}_i - \bar{\boldsymbol{\omega}}^\star_j) + b_i(\bar{\boldsymbol{\omega}}_i - \bar{\boldsymbol{\omega}}_l) \end{cases} \tag{9}$$

It is worth noting that in networked systems with fading channels, where the quality of communication links fluctuates over time, the graph structure plays a crucial role in convergence rates. To mitigate fading channels' impact on the convergence rate of the tracking errors, we involved the expectation of the random variable in Eq. 8 to improve the accuracy of the calculation of the shared information between vehicles and improve the convergence rate of the tracking errors.

Remark 4 *In practice, many factors can contribute to the fading of channels, including time, radio frequency, geographical location, etc. Accordingly, fading can be viewed as a random variation in the transmitted signal's amplitude and phase over time as presented in Eq. 8. This concept can be extended to large-scale systems, presuming that all followers experience the fading channel phenomenon. It is important to note that in Eq. 8, the variable δ_{ij} is not estimated. Instead, the expectation of this random variable is utilized to accurately calculate the tracking errors between one follower and another. In the scenario where δ_{ij} adheres to a Gaussian distribution featuring a central parameter denoted by its mean value $\delta^\star$, the value is highly likely to fall within the range of* *the mean. Consequently, the utilization of the mathematical expectation expression is deemed to augment the precision of computations.*

For the sake of analytical simplification, we introduce the vector $\boldsymbol{\alpha}_i$, characterized by a single non-zero entry in its i^{th} position and zeros elsewhere. Consequently, Eq. 9 can be succinctly reformulated as follows:

$$\begin{cases} \boldsymbol{\varepsilon}^{\star}{}_1 &= (\boldsymbol{L_m} + \boldsymbol{B}) \otimes \boldsymbol{I_m} \sum_{i=1}^{N} \Big(\frac{1}{\delta^{\star}} \boldsymbol{\Pi}_i (\boldsymbol{p} - \boldsymbol{\alpha}_i \otimes (\boldsymbol{p}_i - \boldsymbol{\Delta}_{ij})) \\ & \quad + \boldsymbol{\alpha}_i \otimes (\boldsymbol{p}_i - \boldsymbol{\Delta}_{ij}) - \boldsymbol{1}_N \otimes (\boldsymbol{p}_l - \boldsymbol{\Delta}_{iL}) \Big) \\ \boldsymbol{\varepsilon}_2^{\star} &= (\boldsymbol{L_m} + \boldsymbol{B}) \otimes \boldsymbol{I_m} \sum_{i=1}^{N} \Big(\frac{1}{\delta^{\star}} \boldsymbol{\Pi}_i (\bar{\boldsymbol{\omega}} - \boldsymbol{\alpha}_i \otimes \bar{\boldsymbol{\omega}}_i) \\ & \quad + \boldsymbol{\alpha}_i \otimes \bar{\boldsymbol{\omega}}_i - \boldsymbol{1}_N \otimes \bar{\boldsymbol{\omega}}_l \Big) \end{cases} \tag{10}$$

where $\boldsymbol{\Pi_1} = \mathrm{diag}[0, \delta_{12}, ..., \delta_{1N}]$, $\boldsymbol{\Pi_2} = \mathrm{diag}[\delta_{21}, 0, ..., \delta_{2N}]$, ..., $\boldsymbol{\Pi_N} = \mathrm{diag}[\delta_{N1}, \delta_{N2}, ..., 0]$ and $\boldsymbol{\Pi_i(p - \alpha_i \otimes p_i)}$ refers to the transmitted state information from team members to i^{th} follower.

Taking the time derivative of Eq. 10, one can get

$$\begin{cases} \dot{\boldsymbol{\varepsilon}}^{\star}{}_1 &= \bar{\boldsymbol{\varepsilon}}_2^{\star} \\ \dot{\boldsymbol{\varepsilon}}^{\star}{}_2 &= (\boldsymbol{L_m} + \boldsymbol{B}) \otimes \boldsymbol{I_m} \Big(\bar{\boldsymbol{H}} - \boldsymbol{1} \otimes \boldsymbol{h}(\boldsymbol{q_l}, \bar{\boldsymbol{\omega}}_l) \\ & \quad + \bar{\boldsymbol{M}}^{-1} \boldsymbol{\tau} - \boldsymbol{1} \otimes \bar{\boldsymbol{M}}^{-1} \boldsymbol{\tau_l} \Big) \end{cases} \tag{11}$$

where $\bar{\boldsymbol{\varepsilon}}_2^{\star} = \boldsymbol{J_{3\times2}} \boldsymbol{\varepsilon}_2^{\star}$, $\quad \bar{\boldsymbol{H}} = \sum_{j=1}^{N} \frac{1}{\delta^{\star}} \boldsymbol{\Pi}_i (\dot{\bar{\boldsymbol{\omega}}} - \boldsymbol{\alpha}_i \otimes \dot{\bar{\boldsymbol{\omega}}}_i) + \boldsymbol{\alpha}_i \otimes \dot{\bar{\boldsymbol{\omega}}}_i$. Then, the goal of Eq. 11 is to achieve that $lim_{t\to\infty} \boldsymbol{\varepsilon}^{\star}{}_1 = 0$ and $lim_{t\to\infty} \boldsymbol{\varepsilon}^{\star}{}_2 = 0$.

2.4 Modelling of actuator faults

Actuator faults are recognized as among the most formidable challenges to mitigate within the spectrum of potential system malfunctions. Such faults can significantly impair system performance and precipitate catastrophic incidents. Hence, this study aims to analyze the performance of follower agents affected by multiplicative and additive actuator faults. This investigation is conducted based on the following assumption:

Assumption 3 *[44] There are two types of faults, namely the multiplicative actuator fault denoted by $\boldsymbol{\gamma_i}(t)$ and additive actuator fault denoted by $\boldsymbol{\vartheta_i}(t)$. All of these fault types are restricted within finite boundaries, and their derivatives are existed and bounded as well. Furthermore, we have $\boldsymbol{\vartheta_i} \le \bar{\boldsymbol{\vartheta}}_i$ where $\bar{\boldsymbol{\vartheta}}_i$ is a known bound.*

Given Assumption 3, the actuator faults outlined in Eq. 2 can be represented by the following model:

$$\boldsymbol{\tau_i} = (\boldsymbol{1} - \boldsymbol{\gamma_i}(\boldsymbol{t}))\boldsymbol{\tau_N} + \boldsymbol{\vartheta_i}(\boldsymbol{t}) \tag{12}$$

where $\boldsymbol{\vartheta_i}(t) \in \mathbb{R}^2$, $\boldsymbol{\gamma_i(t)} \in \mathbb{R}^{2\times2}$, with $\boldsymbol{\gamma_i}(t) = \mathrm{diag}([\gamma_1(t), \gamma_2(t)])$, and $0 < \boldsymbol{\gamma_i}(t) \le 1$. $\boldsymbol{\tau_N}$ denotes the nominal torque inputs. It is believed that in the fault-free condition, all the elements of $\gamma_i(t) and \vartheta_i(t)$ equal zero.

3 Main Results

3.1 ANFTSMC design under the impact of fading channels and external disturbances

This section is dedicated to developing an adaptive fault-tolerant controller aimed at preserving the team's stability under the influence of deteriorated neighborhood information. We employ a non-singular fast terminal sliding mode surface to avoid singularities and achieve convergence in a short time. The surface of sliding mode control for the i^{th} follower is chosen as follows:

$$\boldsymbol{s}_i = \boldsymbol{\varepsilon}_{1i}^{\star} + \boldsymbol{K}_{1i}(\boldsymbol{\varepsilon}_{1i}^{\star})^{\eta_1} + \boldsymbol{K}_{2i}(\boldsymbol{\varepsilon}_{2i}^{\star})^{\eta_2} \tag{13}$$

where $\boldsymbol{K}_{1i} > 0$ and $\boldsymbol{K}_{2i} > 0$, then, Eq. 13 can be expressed in compact form as follows:

$$\boldsymbol{s} = \boldsymbol{\varepsilon}_1^{\star} + \boldsymbol{K}_1(\boldsymbol{\varepsilon}_1^{\star})^{\eta_1} + \boldsymbol{K}_2(\varepsilon_2^{\star})^{\eta_2} \tag{14}$$

with

$$\boldsymbol{s} = [s_i^T, s_2^T, ..., s_N^T]$$

Taking the differentiation of Eq. 14 yields:

$$\begin{aligned} \dot{s} &= \dot{\boldsymbol{\varepsilon}}_1^{\star} + \boldsymbol{K}_1\boldsymbol{\Lambda}_1 \mathrm{diag}(|\boldsymbol{\varepsilon}_1^{\star}|^{\eta_1-1})\dot{\boldsymbol{\varepsilon}}_1^{\star} + \boldsymbol{K}_2\boldsymbol{\Lambda}_2 \mathrm{diag}(|\boldsymbol{\varepsilon}_2^{\star}|^{\eta_2-1})\dot{\boldsymbol{\varepsilon}}_2^{\star} \\ &= \boldsymbol{J_{3\times2}}\boldsymbol{\varepsilon}_2^{\star} + \boldsymbol{K}_1\boldsymbol{\Lambda}_1 \mathrm{diag}(|\boldsymbol{\varepsilon}_1^{\star}|^{\eta_1-1})\boldsymbol{J_{3\times2}}\boldsymbol{\varepsilon}_2^{\star} + \boldsymbol{K}_2\boldsymbol{\Lambda}_2 \mathrm{diag}(|\boldsymbol{\varepsilon}_2^{\star}|^{\eta_2-1})\dot{\boldsymbol{\varepsilon}}_2^{\star} \\ &= (\boldsymbol{I} + \boldsymbol{K}_1\boldsymbol{\Lambda}_1 \mathrm{diag}(|\boldsymbol{\varepsilon}_1^{\star}|^{\eta_1-1})\bar{\boldsymbol{\varepsilon}}_2^{\star} + \boldsymbol{K}_2\boldsymbol{\Lambda}_2 \mathrm{diag}(|\boldsymbol{\varepsilon}_2^{\star}|^{\eta_2-1})\dot{\boldsymbol{\varepsilon}}_2^{\star} \end{aligned} \tag{15}$$

where $\boldsymbol{\Lambda_1} = \mathrm{diag}(\eta_1)$ and $\boldsymbol{\Lambda_2} = \mathrm{diag}(\eta_2)$ and $|\boldsymbol{\varepsilon}_1^{\star}|^{\eta_1-1} = (|\boldsymbol{\varepsilon}_{11}^{\star}|^{\eta_{11}-1T}, |\boldsymbol{\varepsilon}_{12}^{\star}|^{\eta_{12}-1T}, ..., |\boldsymbol{\varepsilon}_{1N}^{\star}|^{\eta_{1N}-1T})^T$ and $|\boldsymbol{\varepsilon}_2^{\star}|^{\eta_2-1} = (|\boldsymbol{\varepsilon}_{21}^{\star}|^{\eta_{21}-1T}, |\boldsymbol{\varepsilon}_{22}^{\star}|^{\eta_{22}-1T}, ..., |\boldsymbol{\varepsilon}_{2N}^{\star}|^{\eta_{2N}-1T})^T$.

The ANFTSMC can be formulated for a collective of vehicles in the presence of fading channels as follows:

$$\begin{aligned} \boldsymbol{\tau} &= \bar{\boldsymbol{M}}(\boldsymbol{L_m} + \boldsymbol{B})^{-1} \otimes \boldsymbol{I_m} \mathrm{diag}(\boldsymbol{\varepsilon}_2^{\star}|^{1-\eta_2})(\boldsymbol{K_2\Lambda_2})^{-1} \\ & \quad \times \Big(-(\boldsymbol{I} + \boldsymbol{K_1\Lambda_1} \times \mathrm{diag}(|\boldsymbol{\varepsilon}_1^{\star}|^{\eta_1-1}))\bar{\boldsymbol{\varepsilon}}_2^{\star} \\ & \quad + \boldsymbol{\Upsilon}(s) - \boldsymbol{K}_3 s^{\nu_1} - \boldsymbol{K}_4 s^{\nu_2} \Big) + \boldsymbol{1}_N \otimes \boldsymbol{\tau_l} \end{aligned} \tag{16}$$

where $\boldsymbol{\Upsilon(s)} = [\upsilon(s_1), \upsilon(s_2), ..., \upsilon(s_N)]$ and $\boldsymbol{\upsilon(s_i)}$ is the smoothing function defined in Eq. 18. $\boldsymbol{K}_3$ and $\boldsymbol{K}_4$ are positive gains. By choosing a substantial switching gain, cooperative tracking, as described in Eq. 17, can be attained. However, this approach may lead to severe chattering of actuators and increased energy usage in real applications. Hence, the adaptive mechanism is used to overcome this issue by computing the switching gain σ_i as follows:

$$\dot{\boldsymbol{\sigma}}_i = \boldsymbol{\mu}(\|\boldsymbol{s}_i\| - \boldsymbol{\kappa}\boldsymbol{\sigma}_i) \tag{17}$$

where $\boldsymbol{\mu} > 0$ and $\boldsymbol{\kappa} > 0$. The term $-\kappa\sigma_i$ is used to limit the growth of $\dot{\sigma}_i$.

From Eq. 17, the smoothing function can be written as follows:

$$\boldsymbol{v}(\boldsymbol{s}_i) = \begin{cases} -2\sigma_i \frac{si}{\|s_i\|} & \text{if} \quad \sigma_i \|s_i\| \geq \chi \\ -2\sigma_i \frac{si}{\chi} & \text{if} \quad \sigma_i \|s_i\| < \chi \end{cases} \tag{18}$$

where $\chi > 0$, and σ_i is computed by the adaptive law in Eq. 17.

Theorem 1 *Considering the system introduced in (2) and (3), subject to the effects of fading channels, the utilization of the control law defined in Eq. 16 facilitates the convergence of the tracking error variables presented in Eq. 11 to zero in a finite-time.*

Proof Let us consider the candidate Lyapunov function as follows:

$$V_1 = \frac{1}{2}\boldsymbol{s}^T\boldsymbol{s} + \frac{1}{2\boldsymbol{\mu}}\sum_{i=1}^{N}(\boldsymbol{\sigma}_i - \bar{\boldsymbol{\sigma}})^2 + \frac{1}{2\boldsymbol{\mu}}\sum_{i=1}^{N}\boldsymbol{\sigma}_i^2 \tag{19}$$

where $\bar{\sigma}_i$ is the upper bound of σ_i. A $\bar{\sigma}_i$ is designed to be $\bar{\sigma}_i > \varphi + \sigma_0$, and $\sigma_0 > 0$.

The derivative of Eq. 19 can be given by:

$$\dot{V}_1 = \boldsymbol{s}^T\Big((\boldsymbol{I} + \boldsymbol{K}_1\boldsymbol{\Lambda}_1\text{diag}(|\boldsymbol{\varepsilon}_1^\star|^{\eta_1-1}))\bar{\boldsymbol{\varepsilon}}_2^\star + \boldsymbol{K}_2\boldsymbol{\Lambda}_2\text{diag}(|\boldsymbol{\varepsilon}_2^\star|^{\eta_2-1})\dot{\boldsymbol{\varepsilon}}_2^\star\Big) + \sum_{i=1}^{N}(\boldsymbol{\sigma}_i - \bar{\boldsymbol{\sigma}})(\|\boldsymbol{s}_i\| - \boldsymbol{\kappa}\boldsymbol{\sigma}_i) + \sum_{i=1}^{N}\boldsymbol{\sigma}_i(\|\boldsymbol{s}_i\| - \boldsymbol{\kappa}\boldsymbol{\sigma}_i) \tag{20}$$

Substituting Eqs. 11 into 20 one has

$$\dot{V}_1 = \boldsymbol{s}^T\Big((\boldsymbol{I} + \boldsymbol{K}_1\boldsymbol{\Lambda}_1\text{diag}(|\boldsymbol{\varepsilon}_1^\star|^{\eta_1-1}))\bar{\boldsymbol{\varepsilon}}_2^\star + \boldsymbol{K}_2\boldsymbol{\Lambda}_2 \text{diag}(|\boldsymbol{\varepsilon}_2^\star|^{\eta_2-1})(\boldsymbol{L_m} + \boldsymbol{B}) \otimes \boldsymbol{I_m}(\bar{\boldsymbol{H}} - \boldsymbol{1} \otimes \boldsymbol{h}(\boldsymbol{q_l}, \bar{\boldsymbol{\omega}}_l, t) + \boldsymbol{d} + \bar{\boldsymbol{M}}^{-1}\boldsymbol{\tau} - \boldsymbol{1} \otimes \bar{\boldsymbol{M}}^{-1}\boldsymbol{\tau}_l)\Big) + \boldsymbol{\Xi}(\boldsymbol{s}_i, \boldsymbol{\sigma}) \tag{21}$$

where

$$\boldsymbol{\Xi}(\boldsymbol{s}_i, \boldsymbol{\sigma}) = \sum_{i=1}^{N}(\boldsymbol{\sigma}_i - \bar{\boldsymbol{\sigma}})(\|\boldsymbol{s}_i\| - \boldsymbol{\kappa}\boldsymbol{\sigma}_i) + \sum_{i=1}^{N}\boldsymbol{\sigma}_i(\|\boldsymbol{s}_i\| - \boldsymbol{\kappa}\boldsymbol{\sigma}_i) \tag{22}$$

Given Assumption 2 and the properties associated with the norm, one can obtain:

$$\begin{aligned} \|\bar{\boldsymbol{H}} - \boldsymbol{1} \otimes \boldsymbol{h}_l\| &= \|(\bar{\boldsymbol{h}}_1(\boldsymbol{q}_1, \bar{\boldsymbol{\omega}}_1, t) - \boldsymbol{h}_l(\boldsymbol{q}_l, \bar{\boldsymbol{\omega}}_l, t))^T, \ldots, (\bar{\boldsymbol{h}}_n(\boldsymbol{q}_n, \bar{\boldsymbol{\omega}}_n, t) - \boldsymbol{h}_l(\boldsymbol{q}_l, \bar{\boldsymbol{\omega}}_l, t))^T\| \\ &\leq \|(\|\bar{\boldsymbol{h}}_1(\boldsymbol{q}_1, \bar{\boldsymbol{\omega}}_1, t) - \boldsymbol{h}_l(\boldsymbol{q}_l, \bar{\boldsymbol{\omega}}_l, t)\|, \ldots, \|(\bar{\boldsymbol{h}}_n(\boldsymbol{q}_n, \bar{\boldsymbol{\omega}}_n, t) - \boldsymbol{h}_l(\boldsymbol{q}_l, \bar{\boldsymbol{\omega}}_l, t)\|)\| \\ &\leq \|(\boldsymbol{\mu}_1\|\boldsymbol{q}_1 - \boldsymbol{q}_l\| + \boldsymbol{\mu}_2\|\bar{\boldsymbol{\omega}}_1 - \bar{\boldsymbol{\omega}}_2\|, \ldots, \boldsymbol{\mu}_1\|\boldsymbol{q}_n - \boldsymbol{q}_l\| + \boldsymbol{\mu}_2\|\bar{\boldsymbol{\omega}}_n - \bar{\boldsymbol{\omega}}_l\|)\| \\ &\leq \|(\boldsymbol{\mu}_1\|\boldsymbol{q}_1 - \boldsymbol{q}_l\|, \ldots, +\|\boldsymbol{q}_n - \boldsymbol{q}_l\|)\| + \boldsymbol{\mu}_2\|(\|\bar{\boldsymbol{\omega}}_1 - \bar{\boldsymbol{\omega}}_2\|, \ldots, \|\bar{\boldsymbol{\omega}}_n - \bar{\boldsymbol{\omega}}_2\|)\| \\ &\leq \boldsymbol{\mu}_1\|\boldsymbol{\varepsilon}_1^\star\| + \boldsymbol{\mu}_2\|\boldsymbol{\varepsilon}_2^\star\| \end{aligned} \tag{23}$$

By leveraging the Kronecker product property, one can derive the following:

$$\begin{aligned} \|(\boldsymbol{L_m} + \boldsymbol{B}) \otimes \boldsymbol{I_m}\| &= \Big[\boldsymbol{\lambda}_m\Big([(\boldsymbol{L_m} + \boldsymbol{B}) \otimes \boldsymbol{I_m}]^T[(\boldsymbol{L_m} + \boldsymbol{B}) \otimes \boldsymbol{I_m}]\Big)\Big]^{\frac{1}{2}} \\ &= [\boldsymbol{\lambda}_m(\boldsymbol{L_m} + \boldsymbol{B})^T(\boldsymbol{L_m} + \boldsymbol{B})]^{\frac{1}{2}} \\ &= \|(\boldsymbol{L_m} + \boldsymbol{B})\| \end{aligned} \tag{24}$$

From Lemma 1, Eqs. 23 and 24, one can have

$$\begin{aligned} \|(\boldsymbol{L_m}+\boldsymbol{B}) \otimes \boldsymbol{I_m}(\bar{\boldsymbol{H}} - \boldsymbol{1} \otimes \boldsymbol{h}_l)\| &\leq \|\boldsymbol{L_m} + \boldsymbol{B}\|(\boldsymbol{\mu}_1\|\boldsymbol{\varepsilon}_1^\star\| + \boldsymbol{\mu}_2\|\boldsymbol{\varepsilon}_2^\star\|) \\ &\leq \|\boldsymbol{L_m} + \boldsymbol{B}\|\|\boldsymbol{L_m} + \boldsymbol{B}\|^{-1}(\boldsymbol{\mu}_1\|\boldsymbol{\varepsilon}_1^\star\| + \boldsymbol{\mu}_2\|\boldsymbol{\varepsilon}_2^\star\|) \leq \boldsymbol{\zeta}\boldsymbol{\mu}_1\|\boldsymbol{\varepsilon}_1^\star\| + \boldsymbol{\zeta}\boldsymbol{\mu}_2\|\boldsymbol{\varepsilon}_2^\star\| \end{aligned} \tag{25}$$

By means of Eqs. 24 and 25, one then has

$$\dot{V}_1 = \boldsymbol{s}^T\Big((\boldsymbol{I} + \boldsymbol{K}_1\boldsymbol{\Lambda}_1\text{diag}(|\boldsymbol{\varepsilon}_1^\star|^{\eta_1-1}))\bar{\boldsymbol{\varepsilon}}_2^\star + \boldsymbol{K}_2\boldsymbol{\Lambda}_2 \text{diag}(\boldsymbol{\varepsilon}_2^\star|^{\eta_2-1})(\boldsymbol{\zeta}\boldsymbol{\mu}_1\|\boldsymbol{\varepsilon}_1^\star\| + \boldsymbol{\zeta}\boldsymbol{\mu}_2\|\boldsymbol{\varepsilon}_2^\star\|) + \boldsymbol{K}_2\boldsymbol{\Lambda}_2 \text{diag}(|\boldsymbol{\varepsilon}_2^\star|^{\eta_2-1})(\boldsymbol{L_m} + \boldsymbol{B}) \otimes \boldsymbol{I_m}(\bar{\boldsymbol{M}}^{-1}\boldsymbol{\tau} - \boldsymbol{1} \otimes \bar{\boldsymbol{M}}^{-1}\boldsymbol{\tau}_l + \sqrt{N}\bar{\boldsymbol{d}})\Big) + \boldsymbol{\Xi}(\boldsymbol{s}_i, \boldsymbol{\sigma}) \tag{26}$$

By replacing Eqs. 16 into 26, the following inequality holds:

$$\dot{V}_1 \leq \boldsymbol{K}_2\boldsymbol{\Lambda}_2\text{diag}(|\boldsymbol{\varepsilon}_2^\star|^{\eta_2-1})\Big[(\boldsymbol{\zeta}(\boldsymbol{\mu}_1\|\boldsymbol{\varepsilon}_1^\star\| + \boldsymbol{\mu}_2\|\boldsymbol{\varepsilon}_2^\star\|) + \|\boldsymbol{L_m} + \boldsymbol{B}\|\sqrt{N}\bar{\boldsymbol{d}}\Big]\|\boldsymbol{s}\| - (\boldsymbol{K}_3\boldsymbol{s}^{\nu_1} + \boldsymbol{K}_4\boldsymbol{s}^{\nu_2})\|\boldsymbol{s}\| + \boldsymbol{s}^T\boldsymbol{\Upsilon}(s) + \boldsymbol{\Xi}(\boldsymbol{s}_i, \boldsymbol{\sigma}) \tag{27}$$

We will consider two cases to begin our theoretical analysis:

First, when $\boldsymbol{\sigma}_i\|\boldsymbol{s}_i\| \geq \boldsymbol{\chi}$, $\forall i = 1,..., N$, $s^T\boldsymbol{\Upsilon}(s) = -\sum_{i=1}^{N}\boldsymbol{\sigma}_i\|\boldsymbol{s}_i\|$. Thus, Eq. 27 can be rewritten as follows:+

$$\dot{V}_1 \leq \boldsymbol{\varphi}\|\boldsymbol{s}\| + \boldsymbol{\Xi}(\boldsymbol{s}_i, \boldsymbol{\sigma}) - 2\sum_{i=1}^{N}\boldsymbol{\sigma}_i\|\boldsymbol{s}_i\| - \boldsymbol{K}_3\sum_{i=1}^{N}\|\boldsymbol{s}_i\|^{\nu_{1i}+1} \\ -\boldsymbol{K}_4\sum_{i=1}^{N}\|\boldsymbol{s}_i\|^{\nu_{2i}+1} \tag{28}$$

where $\boldsymbol{\varphi} = \boldsymbol{K}_2\boldsymbol{\Lambda}_2\mathrm{diag}(|\boldsymbol{\varepsilon}_2^\star|^{\eta_2-1})\Big(\boldsymbol{\zeta}(\boldsymbol{\mu}_1\|\boldsymbol{\varepsilon}_1^\star\| + \boldsymbol{\mu}_2\|\boldsymbol{\varepsilon}_2^\star\|) + \|(\boldsymbol{L_m} + \boldsymbol{B})\|\sqrt{N}\bar{\boldsymbol{d}}\Big)$. From Eq. 22, one can write

$$\begin{aligned}\boldsymbol{\Xi}(\boldsymbol{s}_i, \boldsymbol{\sigma}_i) &= 2\sum_{i=1}^{N}\boldsymbol{\sigma}_i\|\boldsymbol{s}_i\| - \boldsymbol{\kappa}\sum_{i=1}^{N}(\boldsymbol{\sigma}_i - \bar{\boldsymbol{\sigma}})\boldsymbol{\sigma}_i - \boldsymbol{\kappa}\sum_{i=1}^{N}(\boldsymbol{\sigma}_i)^2 - \bar{\boldsymbol{\sigma}}\sum_{i=1}^{N}\|\boldsymbol{s}_i\| \\ &= 2\sum_{i=1}^{N}\boldsymbol{\sigma}_i\|\boldsymbol{s}_i\| + \boldsymbol{\kappa}\bar{\boldsymbol{\sigma}}\sum_{i=1}^{N}\boldsymbol{\sigma}_i - 2\boldsymbol{\kappa}\sum_{i=1}^{N}(\boldsymbol{\sigma}_i)^2 - \bar{\boldsymbol{\sigma}}\sum_{i=1}^{N}\|\boldsymbol{s}_i\|\end{aligned} \tag{29}$$

By substituting Eqs. 29 into 28, one can get that

$$\dot{V}_1 \leq -(\bar{\boldsymbol{\sigma}} - \boldsymbol{\varphi})\|\boldsymbol{s}\| + \boldsymbol{\kappa}\bar{\boldsymbol{\sigma}}\sum_{i=1}^{N}\boldsymbol{\sigma}_i - 2\boldsymbol{\kappa}\sum_{i=1}^{N}(\boldsymbol{\sigma}_i)^2 \\ -(\boldsymbol{K}_3 + \boldsymbol{K}_4)\sum_{i=1}^{N}\|\boldsymbol{s}_i\|^{\bar{\nu}+1} \tag{30}$$

Considering that $\boldsymbol{\sigma}_i$ attains its peak when $\sigma_i = \bar{\sigma}$, one can get that

$$\dot{V}_1 \leq -(\boldsymbol{\sigma}_o)\|\boldsymbol{s}\| + \boldsymbol{\rho}_1 \tag{31}$$

with $\boldsymbol{\rho}_1 = -\boldsymbol{\kappa}N\bar{\boldsymbol{\sigma}}^2 - (\boldsymbol{K}_3 + \boldsymbol{K}_4)\sum_{i=1}^{N}\|\boldsymbol{s}_i\|^{\bar{\nu}+1}$.

Second, when $\boldsymbol{\sigma}_i\|\boldsymbol{s}_i\| < \boldsymbol{\chi}$, $\forall\ i = 1,..., N$, $\boldsymbol{s}^T\boldsymbol{\Upsilon}(s) = \sum_{i=1}^{N}\frac{\boldsymbol{\sigma}}{\boldsymbol{\chi}}\|\boldsymbol{s}_i\|$. It follows from Eq. 27 that

$$\begin{aligned}\dot{V}_1 &\leq \boldsymbol{\varphi}\|\boldsymbol{s}\| + \sum_{i=1}^{N}(\boldsymbol{\sigma}_i - \bar{\boldsymbol{\sigma}})(\|\boldsymbol{s}_i\| - \boldsymbol{\kappa}\boldsymbol{\sigma}_i) - \sum_{i=1}^{N}\frac{\boldsymbol{\sigma_i}}{\boldsymbol{\chi}}\|\boldsymbol{s}_i\| \\ &\leq -(\boldsymbol{\sigma}_o)\|\boldsymbol{s}\| - \boldsymbol{\rho}_1 - \boldsymbol{\sigma}_i\sum_{i=1}^{N}(\frac{\mathbf{1}}{\boldsymbol{\chi}} - \boldsymbol{\sigma}_i)\|\boldsymbol{s}_i\| \\ &\leq -(\boldsymbol{\sigma}_o)\|\boldsymbol{s}\| - \boldsymbol{\rho}_2\end{aligned} \tag{32}$$

with $\boldsymbol{\rho}_2 = \boldsymbol{\rho}_1 + \boldsymbol{\sigma}_i\sum_{i=1}^{N}(\frac{\mathbf{1}}{\boldsymbol{\chi}} + \boldsymbol{\sigma}_i)\|\boldsymbol{s}_i\|$.

The following inequality holds when Cases I and II are combined as follows:

$$\begin{aligned}\dot{V}_1 &\leq -(\boldsymbol{\sigma}_o)\|\boldsymbol{s}\| + \boldsymbol{\rho} \\ &\leq -(1 - \Omega)\boldsymbol{\sigma}_0\|\boldsymbol{s}\|\end{aligned} \tag{33}$$

where $\boldsymbol{\rho}$ represents the maximum value between ρ_1 and ρ_2, with Ω constrained within the range $0 < \Omega < 1$. As a result, the sliding manifold s will converge to the boundary layer $\bar{\theta}_1$ in a finite time.

$$\bar{\theta}_1 = \left\{\|s\| \leq \frac{\sigma}{\Omega\sigma_0}\right\} \tag{34}$$

The property of ultimate boundedness exhibited by s entails that $\varepsilon_1^\star$ and $\varepsilon_2^\star$ are bounded. Hence, based on Definition 1 and Remark 2, it can be inferred that the CUUB criterion is met. This concludes the proof. □

3.2 ANFTSMC design under the impact of actuator faults, fading channels, and external disturbances

This section presents a consensus algorithm for multiple vehicles affected by actuator faults, fading channels, and external disturbances.

Theorem 2 *The implementation of the Cooperative Uniform Ultimate Boundedness (CUUB) approach for a group of vehicles encountering actuator faults, random fading signals, and external disturbances is attainable through the utilization of the control law in Eq. 16 and the adaptive mechanism in Eq. 17 under the condition that*

$$\boldsymbol{\epsilon} = (\boldsymbol{L_m} + \boldsymbol{B})\bar{\boldsymbol{\gamma}}(\boldsymbol{L_m} + \boldsymbol{B})^{-1} \tag{35}$$

where $\boldsymbol{\epsilon} > 0$ and $\bar{\boldsymbol{\gamma}} = diag\{\gamma_1(t), ..., \gamma_N(t)\}$.

Proof Consider the following candidate Lyapunov function:

$$V_1 = \frac{1}{2}\boldsymbol{s}^T\boldsymbol{s} + \frac{\boldsymbol{\epsilon}}{2\boldsymbol{\mu}}\sum_{i=1}^{N}((\boldsymbol{\sigma}_i - \bar{\boldsymbol{\sigma}})^2 + \boldsymbol{\sigma}_i^2) \tag{36}$$

we assume that $\bar{\boldsymbol{\sigma}} > \boldsymbol{\varphi}' + \boldsymbol{\sigma}_o'$, where, $\boldsymbol{\varphi}'$ will be explicitly defined at a later stage, and $\boldsymbol{\sigma}_o'$ is stipulated to be greater than zero.

By computing the time derivative of Eq. 36 and utilizing equations Eqs. 11, 12 and 25, one can obtain

$$\begin{aligned}\dot{V}_1 = \boldsymbol{s}^T\Big(&(\boldsymbol{I} + \boldsymbol{K}_1\boldsymbol{\Lambda}_1\mathrm{diag}(|\boldsymbol{\varepsilon}_1^\star|^{\eta_1-1}))\bar{\boldsymbol{\varepsilon}}_2^\star + \boldsymbol{K}_2\boldsymbol{\Lambda}_2. \\ &\mathrm{diag}(|\boldsymbol{\varepsilon}_2^\star|^{\eta_2-1})(\boldsymbol{\zeta}\boldsymbol{\mu}_1\|\boldsymbol{\varepsilon}_1^\star\| + \boldsymbol{\zeta}\boldsymbol{\mu}_2\|\boldsymbol{\varepsilon}_2^\star\|) + \boldsymbol{K}_2\boldsymbol{\Lambda}_2 \\ &\mathrm{diag}(|\boldsymbol{\varepsilon}_2^\star|^{\eta_2-1})(\boldsymbol{L_m} + \boldsymbol{B})\boldsymbol{I_m}(\bar{\boldsymbol{M}}^{-1}(\boldsymbol{I} - \boldsymbol{\gamma}_i(t))\boldsymbol{\tau}_N \\ &+\boldsymbol{\vartheta}_i(t) - 1 \otimes \bar{\boldsymbol{M}}^{-1}\boldsymbol{\tau}_l + \sqrt{N}\bar{\boldsymbol{d}})\Big)\boldsymbol{\epsilon}\boldsymbol{\Xi}(\boldsymbol{s}_i, \boldsymbol{\sigma})\end{aligned} \tag{37}$$

By replacing Eqs. 16 and 35 into Eq. 37, one can obtain the following:

$$
\begin{aligned}
\dot{V}_1 &= s^T\Big(\boldsymbol{K}_2\boldsymbol{\Lambda}_2\mathrm{diag}(|\boldsymbol{\varepsilon}_2^\star|^{\eta_2-1}\Big[(\boldsymbol{\zeta}(\boldsymbol{\mu}_1\|\boldsymbol{\varepsilon}_1^\star\|+\boldsymbol{\mu}_2\|\boldsymbol{\varepsilon}_2^\star\|) \\
&\quad +\|\boldsymbol{L_m}+\boldsymbol{B}\|\sqrt{\boldsymbol{N}}\bar{\boldsymbol{d}}+\|\boldsymbol{L_m}+\boldsymbol{B}\|\sqrt{\boldsymbol{N}}\bar{\boldsymbol{\vartheta}}_i\Big] \\
&\quad -(\boldsymbol{K}_3 s^{\nu_1}+\boldsymbol{K}_4 s^{\nu_2})+\boldsymbol{\Upsilon}(s)-\|\boldsymbol{L_m}+\boldsymbol{B}\|\bar{\boldsymbol{\gamma}}\|\boldsymbol{L_m}+\boldsymbol{B}\|^{-1} \\
&\quad \otimes\boldsymbol{I_m}\Big[\boldsymbol{b}\otimes\bar{\boldsymbol{M}}^{-1}\boldsymbol{\tau}_l-(\boldsymbol{I}+\boldsymbol{K}_1\boldsymbol{\Lambda}_1\mathrm{diag}(|\boldsymbol{\varepsilon}_1^\star|^{\eta_1-1}))\bar{\boldsymbol{\varepsilon}}_2^\star\boldsymbol{\Upsilon}(s) \\
&\quad -\boldsymbol{K}_3\boldsymbol{s}^{\nu_1}-\boldsymbol{K}_4\boldsymbol{s}^{\nu_2}\Big]\Big)+\boldsymbol{\epsilon}\,\boldsymbol{\Xi}(\boldsymbol{s}_i,\boldsymbol{\sigma}) \\
&\le \boldsymbol{K}_2\boldsymbol{\Lambda}_2\mathrm{diag}(|\boldsymbol{\varepsilon}_2^\star|^{\eta_2-1}\Big[(\boldsymbol{\zeta}(\boldsymbol{\mu_1}\|\boldsymbol{\varepsilon}_1^\star\|+\boldsymbol{\mu}_2\|\boldsymbol{\varepsilon}_2^\star\|) \\
&\quad +|L_m+B\|.\sqrt{\boldsymbol{N}}\bar{\boldsymbol{d}}\Big]\|\boldsymbol{s}\|-\|\boldsymbol{L_m}+\boldsymbol{B}\|\bar{\boldsymbol{\gamma}}\|\boldsymbol{L_m}+\boldsymbol{B}\|^{-1} \\
&\quad \otimes\boldsymbol{I_m}\Big[\boldsymbol{b}\otimes\bar{\boldsymbol{M}}^{-1}\boldsymbol{\tau}_l-(\boldsymbol{I}+\boldsymbol{K}_1\boldsymbol{\Lambda}_1\mathrm{diag}(|\boldsymbol{\varepsilon}_1^\star|^{\eta_1-1})) \\
&\quad \bar{\varepsilon}_2^\star\Big]\|s\| -\boldsymbol{\epsilon}\boldsymbol{s}^T(\boldsymbol{K}_3\boldsymbol{s}^{\nu_1}+\boldsymbol{K}_4\boldsymbol{s}^{\nu_2})+\boldsymbol{\epsilon}\boldsymbol{s}^T\boldsymbol{\Upsilon}(s) \\
&\quad +\|\boldsymbol{L_m}+\boldsymbol{B}\|\sqrt{\boldsymbol{N}}\bar{\boldsymbol{\vartheta}}\|\boldsymbol{s}\|+\boldsymbol{\epsilon}\,\boldsymbol{\Xi}(\boldsymbol{s}_i,\boldsymbol{\sigma}) \\
&\le \boldsymbol{\varphi}'\|\boldsymbol{s}\|+\boldsymbol{\epsilon}\boldsymbol{s}^T\boldsymbol{\Upsilon}(s)-\boldsymbol{\epsilon}\boldsymbol{s}^T(\boldsymbol{K}_3\boldsymbol{s}^{\nu_1}+\boldsymbol{K}_4\boldsymbol{s}^{\nu_2}) \\
&\quad +\boldsymbol{\epsilon}\,\boldsymbol{\Xi}(\boldsymbol{s}_i,\boldsymbol{\sigma})
\end{aligned} \tag{38}
$$

where $\boldsymbol{\varphi}'=\boldsymbol{\varphi}-\|\boldsymbol{L_m}+\boldsymbol{B}\|\bar{\boldsymbol{\gamma}}\|\boldsymbol{L_m}+\boldsymbol{B}\|^{-1}\otimes\boldsymbol{I_m}.\Big[\boldsymbol{b}\otimes\bar{\boldsymbol{M}}^{-1}\boldsymbol{\tau}_l-(\boldsymbol{I}+\boldsymbol{K}_1\boldsymbol{\Lambda}_1\mathrm{diag}(|\boldsymbol{\varepsilon}_1^\star|^{\eta_1-1}))\bar{\boldsymbol{\varepsilon}}_2^\star\Big]+\|\boldsymbol{L_m}+\boldsymbol{B}\|\sqrt{\boldsymbol{N}}\bar{\boldsymbol{\vartheta}}$

Now, let's consider that when $\boldsymbol{\sigma}_i\|\boldsymbol{s}_i\|\ge\boldsymbol{\chi}$, $\forall_i=1,..,N$, $\boldsymbol{s}^T\boldsymbol{\Upsilon}(s)=\sum_{i=1}^N\boldsymbol{\sigma}\|\boldsymbol{s}_i\|$.

$$
\begin{aligned}
\dot{V}_1 &\le \boldsymbol{\varphi}'\|\boldsymbol{s}\|-\boldsymbol{\epsilon}\bar{\boldsymbol{\sigma}}\sum_{i=1}^N\|\boldsymbol{s}_i\|+\boldsymbol{\epsilon}\Big[\boldsymbol{\kappa}\bar{\boldsymbol{\sigma}}\sum_{i=1}^N\boldsymbol{\sigma}_i-2\boldsymbol{\kappa}\sum_{i=1}^N(\boldsymbol{\sigma}_i)^2 \\
&\quad -(\boldsymbol{K}_3+\boldsymbol{K}_4)\sum_{i=1}^N\|\boldsymbol{s}_i\|^{\bar{\nu}+1}\Big] \\
&\le -(\boldsymbol{\sigma}_o')\|\boldsymbol{s}\|+\boldsymbol{\epsilon}\boldsymbol{\rho}_1
\end{aligned} \tag{39}
$$

Second, when $\boldsymbol{\sigma}_i\|\boldsymbol{s}_i\|<\boldsymbol{\chi}$, $\forall_i=1,\ldots,N$, $\boldsymbol{s}^T\boldsymbol{\Upsilon}(s)=\sum_{i=1}^N\frac{\boldsymbol{\sigma}}{\boldsymbol{\chi}}\|\boldsymbol{s_i}\|$.

$$
\begin{aligned}
\dot{V}_1 &\le \boldsymbol{\varphi}'\|\boldsymbol{s}\|+\sum_{i=1}^N(\boldsymbol{\sigma}_i-\bar{\boldsymbol{\sigma}})(\|\boldsymbol{s}_i\|-\boldsymbol{\kappa}\boldsymbol{\sigma}_i)-\sum_{i=1}^N\frac{\boldsymbol{\sigma_i}}{\boldsymbol{\chi}}\|\boldsymbol{s_i}\| \\
&\le -(\boldsymbol{\sigma}_o')\|\boldsymbol{s}\|-\boldsymbol{\rho}_1'-\boldsymbol{\sigma}_i\sum_{i=1}^N(\frac{\boldsymbol{1}}{\boldsymbol{\chi}}-\boldsymbol{\sigma}_i)\|\boldsymbol{s}_i\| \\
&\le -(\boldsymbol{\sigma}_o')\|\boldsymbol{s}\|-\boldsymbol{\rho}_2'
\end{aligned} \tag{40}
$$

with $\boldsymbol{\rho}_2'=\boldsymbol{\rho}_1'+\boldsymbol{\sigma}_i\sum_{i=1}^N(\frac{\boldsymbol{1}}{\boldsymbol{\chi}}+\boldsymbol{\sigma}_i)\|\boldsymbol{s}_i\|$.

The following inequality can be obtained by combining Cases I and II:

$$
\begin{aligned}
\dot{V}_1 &\le -(\boldsymbol{\sigma}_o')\|\boldsymbol{s}\|+\boldsymbol{\rho}' \\
&\le -(1-\Omega)\boldsymbol{\sigma}_0'\|\boldsymbol{s}\|
\end{aligned} \tag{41}
$$

Thus, the sliding manifold s will reach the boundary layer $\bar{\theta}_2$ within a finite time.

$$
\bar{\theta}_2=\left\{\|s\|\le\frac{\sigma}{\Omega\sigma_0'}\right\} \tag{42}
$$

Then, the ultimate boundedness property of s implies that $\varepsilon_1^\star$ and $\varepsilon_2^\star$ are confined within finite bounds. Consequently, by Definition 1 and Remark 2, it follows that the tracking error system described in Eq. 11 satisfies the CUUB criterion. This concludes the proof. □

4 Numerical Simulations

Numerical simulations have been performed to examine the effectiveness of the proposed ANFTSMC in manipulating a group of car-like vehicles. The ANFTSMC is adaptable for implementation across various configurations of networked control systems. For instance, Fig. 2 depicts a configuration comprising one leader and four followers, where L denotes the leader, and F1-F4 denotes the four followers. Within the graph structure, F1 and F2 maintain direct connections with the leader. F2 transmits faded state information to F3 and F4 while receiving complete state information from both the leader and F1. Hence, we can describe the relationships as follows:

$$
A=\begin{bmatrix}0&0&0&0\\0&0&0&0\\0&1&0&0\\0&1&0&0\end{bmatrix}\qquad ;L_m=\begin{bmatrix}0&0&0&0\\0&0&0&0\\0&-1&1&0\\0&-1&0&1\end{bmatrix}
$$

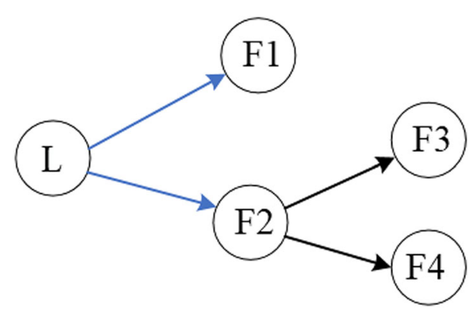

Fig. 2 Communication topology

Table 1 Physical parameters of vehicles

Parameters	Values	Unit
m_c	2.5	(Kg)
m_w	0.23	(Kg)
L	0.2	(m)
$2W$	0.1	(m)
I_{bzz}	0.015	(kgm^2)
I_{wzz}	0.002	(kgm^2)

and the diagonal matrix $B = \text{diag}(1, 1, 0, 0)$.

The parameters of the ANFTSMC in Eq. 16 are chosen as $K_1 = 10$, $K_2 = 5$, $K_3 = 0.5$, $K_4 = 0.5$, $\mu = 2.7$, $\kappa = 0.0025$ and $\xi = 0.0035$. Followers are affected by the following disturbance $d_i = 0.1sin(0.1it + \frac{i}{3}\pi)$. The identical parameters of the vehicles are given in Table 1.

In the simulation, we have examined the performance of the ANFTSMC compared with the results of the Integral Sliding Mode Control (ISMC). In recent years, many researchers have identified ISMC as a potential candidate for the fault-tolerant control design problem due to its inherent capability to handle system uncertainties [45]. In this work, we assume that Follower 2 experiences a fading channel phenomenon from time $t = 0$ second to the time of mission completion. Therefore, throughout the entire operation, Follower 3 and Follower 4 receive faded state information. Additionally, Follower 3 experiences a left actuator fault characterized by $\gamma_i = 0.30$ and $\vartheta_i = 0.5 + 0.2e^{-0.1t}$ (N.m) from time $t = 0$ second up to the end of the mission.

Figure 3 shows the trajectory tracking results of the leader and four followers in the presence of faults using ANFTSMC.

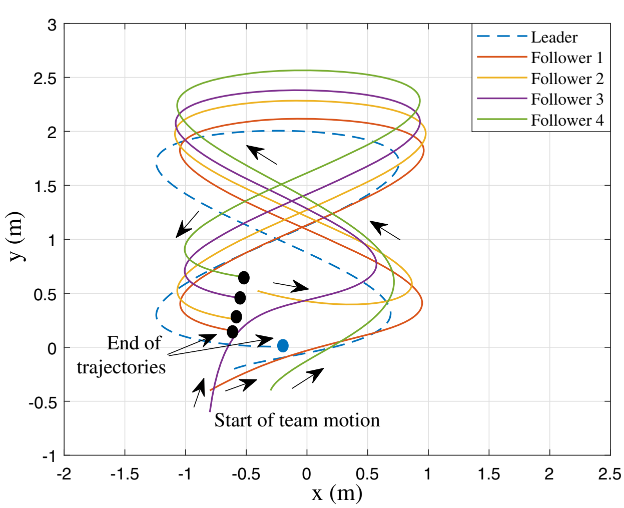

Fig. 3 Actual trajectories of the leader and followers using ANFTSMC

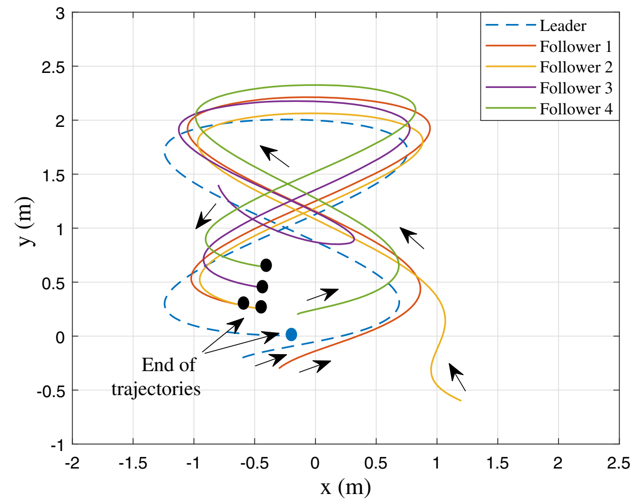

Fig. 4 Actual trajectories of the leader and followers using ISMC

Although F3 and F4 receive faded state information via the fading channel of F2, the expectation of the random variables improved the accuracy of the calculation and enabled the ANFTSMC to cope with the occurrence of faults. Compared with the results of the ISMC in Fig. 4, ANFTSMC provided better performance in manipulating the state information of the followers, enhancing their capabilities to track the reference trajectories more accurately. Although the two controllers steered the followers within approximately similar linear velocity, steering velocity, and orientation as presented in Figs. 5, 6 and 7, it can be observed from Figs. 8 and 9 that the finite-time consensus tracking of the follow-

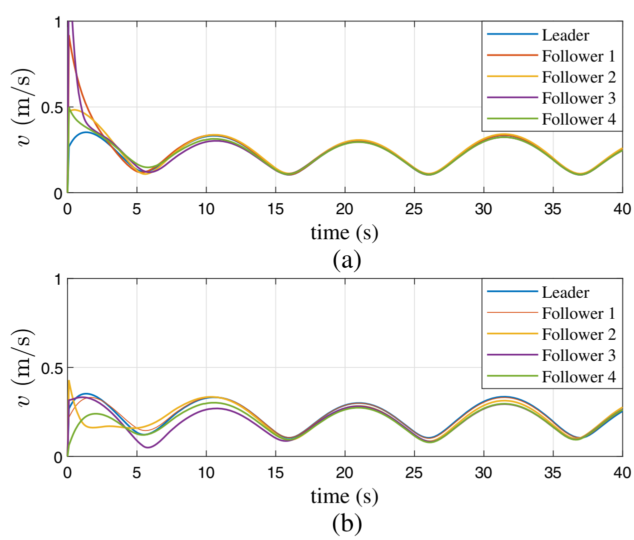

Fig. 5 Consensus of linear velocities. (a) Using ANFTSMC. (b) Using ISMC

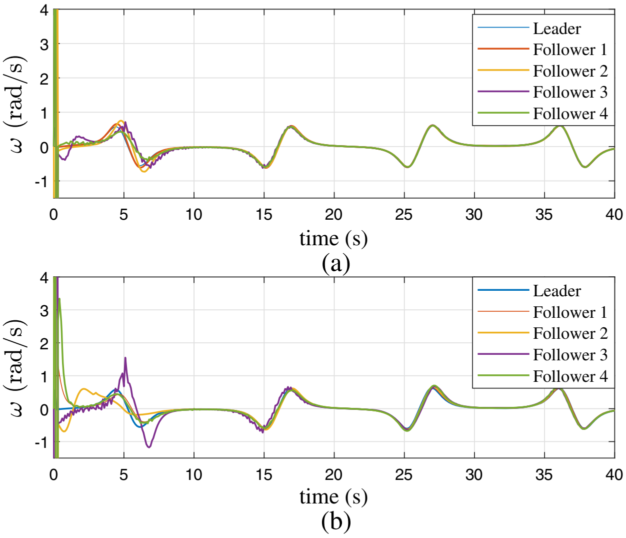

Fig. 6 Consensus of steering velocity. (a) Using ANFTSMC. (b) Using ISMC

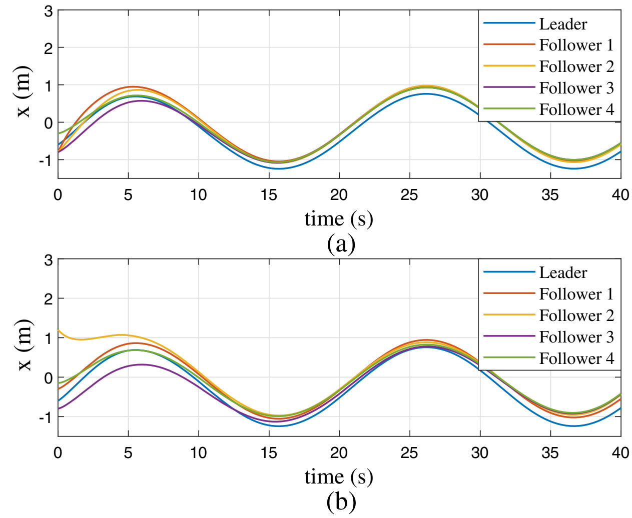

Fig. 8 Consensus of positions. (a) Trajectories tracking on the x-axis using ANFTSMC. (b) Trajectories tracking on the x-axis using ISMC

ers can only be achieved by the proposed ANFTSMC after approximately 10 seconds on the x-axis and 5 seconds on the y-axis while maintaining the required distances between them. Moreover, Figs. 10 and 11 show that the state tracking errors remained in the vicinity of zero and the CUUB of the followers was only achieved by ANFTSMC. These results demonstrate the effectiveness of the proposed ANFTSMC for tackling issues pertaining to faded state information and actuator faults amidst disturbances. Additionally, they verify the theoretical conclusions presented in Theorems 1 and 2.

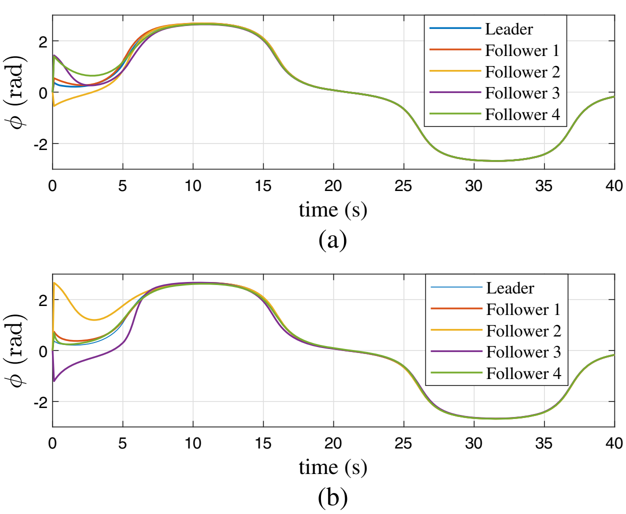

Fig. 7 Consensus of orientations. (a) Using ANFTSMC. (b) Using ISMC

5 Conclusion and Future Work

This paper focuses on developing cooperative control strategies specifically designed for networked control systems facing issues such as fading channels, actuator faults, and external disturbances. A novel control scheme based on the non-singular fast terminal sliding mode control approach is proposed, wherein all follower agents synchronize with the leader, achieving tracking errors that converge to a confined region around the origin. Moreover, it is demonstrated that the

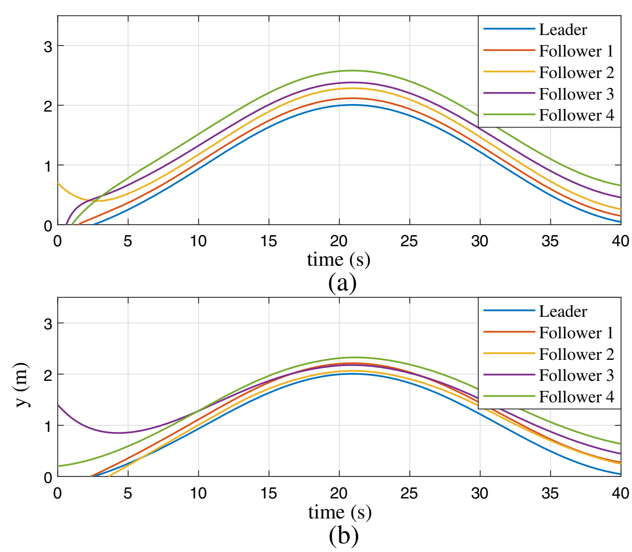

Fig. 9 Consensus of positions. (a) Trajectories tracking on the y-axis using ANFTSMC. (b) Trajectories tracking on the y-axis using ISMC

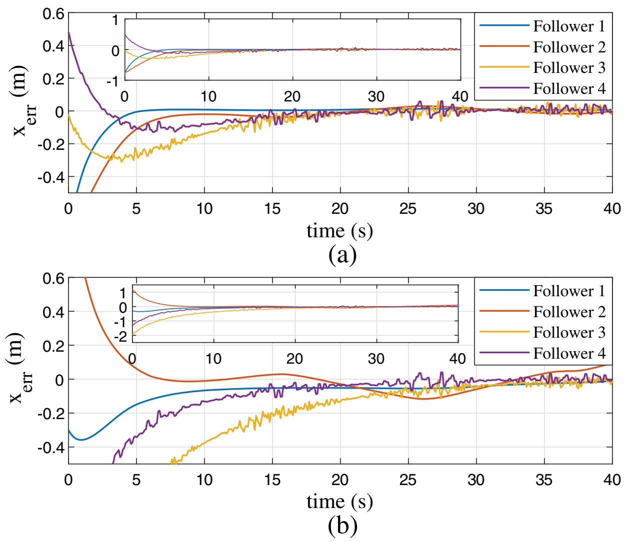

Fig. 10 Position tracking errors on the x-axis. (a) Using ANFTSMC. (b) Using ISMC

tracking errors remain uniformly bounded within a finite time frame. The effectiveness of the proposed ANFTSMC has been verified, showing its ability to operate successfully even in situations where uncertainties or disturbances in the system are not known in advance. In future research endeavors, exploring the cooperative control problem under dynamic communication networks, considering communication and actuator challenges, would be a valuable area for further investigation.

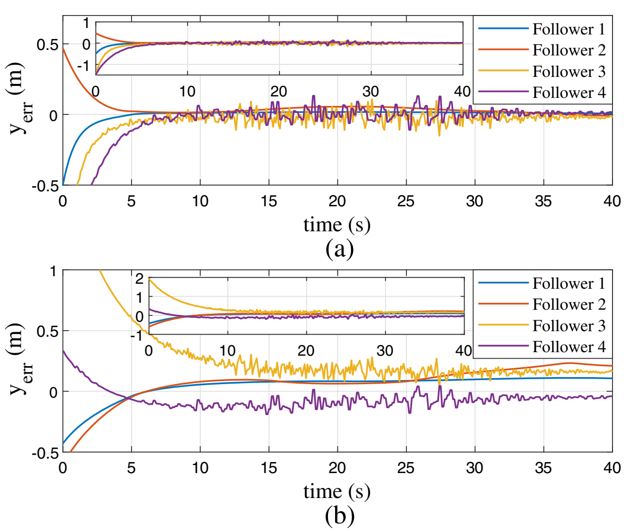

Fig. 11 Position tracking errors on the y-axis. (a) Using ANFTSMC. (b) Using ISMC

Author Contributions Mahmoud Hussein: Conceptualization, Methodology, Validation, Writing the original draft. Youmin Zhang: Supervision, Discussion, Resources, Writing, review and editing. Zhaoheng Liu: Supervision, Discussion, Resources, Writing, review and editing.

Funding This work was supported in part by the Natural Sciences and Engineering Research Council of Canada (NSERC).

Declarations

Conflicts of interest The authors declare that they have no known conflicts of interest/competing interests.

References

1. Hadi, B., Khosravi, A., Sarhadi, P.: A review of the path planning and formation control for multiple autonomous underwater vehicles. Journal of Intelligent & Robotic Systems **101**, 1–26 (2021). https://doi.org/10.1007/s10846-021-01330-4
2. Kamel, M.A., Yu, X., Zhang, Y.: Formation control and coordination of multiple unmanned ground vehicles in normal and faulty situations: A review. Annu. Rev. Control. **49**, 128–144 (2020). https://doi.org/10.1016/j.arcontrol.2020.02.001
3. Yu, H., Chen, X., Chen, T., Hao, F.: Event-triggered bipartite consensus for mul-tiagent systems: A zeno-free analysis. IEEE Trans. Autom. Control **65**(11), 4866–4873 (2019). https://doi.org/10.1109/TAC.2019.2962092
4. Wei, L., Chen, W.-H., Luo, S., Huang, G.: Impulsive average-consensus of multi-agent systems with time-delays. J. Franklin Inst. **359**(2), 1544–1568 (2022). https://doi.org/10.1016/j.jfranklin.2021.11.030
5. Zhang, Z., Chen, S., Zheng, Y.: Leader-following scaled consensus of second-order multi-agent systems under directed topologies. Int. J. Syst. Sci. **50**(14), 2604–2615 (2019). https://doi.org/10.1080/00207721.2019.1672115
6. Lu, M., Wu, J., Zhan, X., Han, T., Yan, H.: Consensus of second-order heterogeneous multi-agent systems with and without input saturation. ISA Trans. **126**, 14–20 (2022). https://doi.org/10.1016/j.isatra.2021.08.001
7. Wu, Z.-G., Xu, Y., Lu, R., Wu, Y., Huang, T.: Event-triggered control for consensus of multiagent systems with fixed/switching topologies. IEEE Transactions on Systems, Man, and Cybernetics: Systems **48**(10), 1736–1746 (2017). https://doi.org/10.1109/TSMC.2017.2744671

8. Ren, Y., Wang, Q., Duan, Z.: Optimal distributed leader-following consensus of linear multi-agent systems: A dynamic average consensus-based approach. IEEE Trans. Circuits Syst. II Express Briefs **69**(3), 1208–1212 (2021). https://doi.org/10.1109/TCSII.2021.3094056
9. Wang, G., Wang, C., Cai, X., Ji, Y.: Distributed leaderless and leader-following consensus control of multiple Euler-Lagrange systems with unknown control directions. Journal of Intelligent & Robotic Systems **89**, 439–463 (2018). https://doi.org/10.1007/s10846-017-0554-1
10. Yaghoubi, Z., Talebi, H.A.: Cluster consensus for nonlinear multi-agent systems. Journal of Intelligent & Robotic Systems **100**(3–4), 1069–1084 (2020). https://doi.org/10.1007/s10846-020-01218-9
11. Cai, J., Wen, C., Su, H., Liu, Z.: Robust adaptive failure compensation of hysteretic actuators for a class of uncertain nonlinear systems. IEEE Trans. Autom. Control **58**(9), 2388–2394 (2013). https://doi.org/10.1109/TAC.2013.2251795
12. Wang, F., Zhang, Y., Zhang, L., Zhang, J., Huang, Y.: Finite-time consensus of stochastic nonlinear multi-agent systems. Int. J. Fuzzy Syst. **22**, 77–88 (2020). https://doi.org/10.1007/s40815-019-00769-w
13. Yu, Z., Zhang, W.: Almost sure consensus of stochastic nonlinear multi-agent systems via event-triggered control. Nonlinear Dyn. **111**(4), 3469–3478 (2023). https://doi.org/10.1007/s11071-022-07999-y
14. Niu, X., Liu, Y., Man, Y.: Finite-time consensus tracking for multi-agent systems with inherent uncertainties and disturbances. Int. J. Control **92**(6), 1415–1425 (2019). https://doi.org/10.1080/00207179.2017.1397289
15. Ren, H., Peng, Y., Deng, F., Zhang, C.: Impulsive pinning control algorithm of stochastic multi-agent systems with unbounded distributed delays. Nonlinear Dyn. **92**, 1453–1467 (2018). https://doi.org/10.1007/s11071-018-4138-9
16. Wu, X., Huang, Y.: Adaptive fractional-order non-singular terminal sliding mode control based on fuzzy wavelet neural networks for omnidirectional mobile robot manipulator. ISA Trans. **121**, 258–267 (2022). https://doi.org/10.1016/j.isatra.2021.03.035
17. Zhang, Y., Yang, X., Wei, P., Liu, P.X.: Fractional-order adaptive non-singular fast terminal sliding mode control with time delay estimation for robotic manipulators. IET Control Theory & Applications **14**(17), 2556–2565 (2020). https://doi.org/10.1049/iet-cta.2019.1302
18. Zhang, X., Quan, Y.: Fractional non-singular fast terminal sliding mode control based on disturbance observer. Internaltional Journal of Innovative Computing, Information and Control 18(1), 93–104 (2022). https://doi.org/10.24507/ijicic.18.01.93
19. Jin, X.-Z., Zhao, Z., He, Y.-G.: Insensitive leader-following consensus for a class of uncertain multi-agent systems against actuator faults. Neurocomputing **272**, 189–196 (2018). https://doi.org/10.1016/j.neucom.2017.06.072
20. Kamel, M.A., Ghamry, K.A., Zhang, Y.: Real-time fault-tolerant cooperative control of multiple UAVs-UGVs in the presence of actuator faults. Journal of Intelligent & Robotic Systems **88**, 469–480 (2017). https://doi.org/10.1007/s10846-016-0463-8
21. Yu, Z., Qu, Y., Zhang, Y.: Fault-tolerant containment control of multiple unmanned aerial vehicles based on distributed sliding-mode observer. Journal of Intelligent & Robotic Systems **93**, 163–177 (2019). https://doi.org/10.1007/s10846-018-0862-0
22. Kheirandish, M., Yazdi, E.A., Mohammadi, H., Mohammadi, M.: A fault-tolerant sensor fusion in mobile robots using multiple model Kalman filters. Robot. Auton. Syst. **161**, 104343 (2023). https://doi.org/10.1016/j.robot.2022.104343
23. Naseri, K., Vu, M.T., Mobayen, S., Najafi, A., Fekih, A.: Design of linear matrix inequality-based adaptive barrier global sliding mode fault tolerant control for uncertain systems with faulty actuators. Mathematics **10**(13), 2159 (2022). https://doi.org/10.3390/math10132159
24. Ju, Y., Tian, X., Liu, H., Ma, L.: Fault detection of networked dynamical systems: A survey of trends and techniques. Int. J. Syst. Sci. **52**(16), 3390–3409 (2021). https://doi.org/10.1080/00207721.2021.1998722
25. Yu, Z., Zhang, Y., Jiang, B., Yu, X.: Fault-tolerant time-varying elliptical formation control of multiple fixed-wing UAVs for cooperative forest fire monitoring. Journal of Intelligent & Robotic Systems **101**, 1–15 (2021). https://doi.org/10.1007/s10846-021-01320-6
26. Xu, Y., Sun, J., Wu, Z.-G., Wang, G.: Fully distributed adaptive event-triggered control of networked systems with actuator bias faults. IEEE Transactions on Cybernetics **52**(10), 10773–10784 (2021). https://doi.org/10.1109/TCYB.2021.3059049
27. Xu, L.-X., Wang, Y.-L., Wang, X., Peng, C.: Decentralized event-triggered adaptive control for interconnected nonlinear systems with actuator failures. IEEE Trans. Fuzzy Syst. **31**(1), 148–159 (2022). https://doi.org/10.1109/TFUZZ.2022.3183798
28. Qu, G., Shen, D., Yu, X.: Batch-based learning consensus of multiagent systems with faded neighborhood information. IEEE Transactions on Neural Networks and Learning Systems (2021). https://doi.org/10.1109/TNNLS.2021.3110684
29. Hu, B.: Stochastic stability analysis for vehicular networked systems with state-dependent bursty fading channels: A self-triggered approach. Automatica **123**, 109352 (2021). https://doi.org/10.1016/j.automatica.2020.109352
30. Shen, D., Qu, G.: Performance enhancement of learning tracking systems over fading channels with multiplicative and additive randomness. IEEE Transactions on Neural Networks and Learning Systems **31**(4), 1196–1210 (2019). https://doi.org/10.1109/TNNLS.2019.2919510
31. Shen, D., Yu, X.: Learning tracking over unknown fading channels based on iterative estimation. IEEE Transactions on Neural Networks and Learning Systems **33**(1), 48–60 (2020). https://doi.org/10.1109/TNNLS.2020.3027475
32. Qu, G., Shen, D.: Stochastic iterative learning control with faded signals. IEEE/CAA Journal of Automatica Sinica **6**(5), 1196–1208 (2019). https://doi.org/10.1109/JAS.2019.1911696
33. Bu, X., Yu, W., Yu, Q., Hou, Z., Yang, J.: Event-triggered model-free adaptive iterative learning control for a class of nonlinear systems over fading channels. IEEE Transactions on Cybernetics **52**(9), 9597–9608 (2021). https://doi.org/10.1109/TCYB.2021.3058997
34. Cao, W., Yan, J., Yang, X., Luo, X., Guan, X.: Communication-aware formation control of AUVs with model uncertainty and fading channel via integral reinforcement learning. IEEE/CAA Journal of Automatica Sinica **10**(1), 159–176 (2023). https://doi.org/10.1109/JAS.2023.123021
35. Wang, X., Zhou, Y., Huang, T., Chakrabarti, P.: Event-triggered adaptive fault tolerant control for a class of nonlinear multiagent systems with sensor and actuator faults. IEEE Trans. Circuits Syst. I Regul. Pap. **69**(10), 4203–4214 (2022). https://doi.org/10.1109/TCSI.2022.3192046
36. Li, Y., Dong, S., Li, K., Tong, S.: Fuzzy adaptive fault tolerant time-varying formation control for nonholonomic multirobot systems with range constraints. IEEE Transactions on Intelligent Vehicles **8**(6), 3668–3679 (2023). https://doi.org/10.1109/TIV.2023.3264800
37. Abci, B., El Badaoui El Najjar, M., Cocquempot, V., Dherbomez, G.: An informational approach for sensor and actuator fault diagnosis for autonomous mobile robots. Journal of Intelligent & Robotic Systems **99**, 387–406 (2020). https://doi.org/10.1007/s10846-019-01099-7
38. Lü, H., He, W., Han, Q.-L., Ge, X., Peng, C.: Finite-time containment control for nonlinear multi-agent systems with external

disturbances. Inf. Sci. **512**, 338–351 (2020). https://doi.org/10.1016/j.ins.2019.05.049
39. Guo, X.-G., Tan, D.-C., Ahn, C.K., Wang, J.-L.: Fully distributed adaptive fault-tolerant sliding-mode control for nonlinear leader-following multiagent systems with ANASs and IQCs. IEEE Transactions on Cybernetics **52**(5), 2763–2774 (2020). https://doi.org/10.1109/TCYB.2020.3023747
40. Gao, Y., Liu, C., Duan, D., Zhang, S.: Distributed optimal event-triggered cooperative control for nonlinear multi-missile guidance systems with partially unknown dynamics. Int. J. Robust Nonlinear Control **32**(15), 8369–8396 (2022). https://doi.org/10.1002/rnc.6285
41. Ren, C.-E., Chen, C.P.: Sliding mode leader-following consensus controllers for second-order non-linear multi-agent systems. IET Control Theory & Applications **9**(10), 1544–1552 (2015). https://doi.org/10.1049/iet-cta.2014.0523
42. Zhang, H., Lewis, F.L.: Adaptive cooperative tracking control of higher-order nonlinear systems with unknown dynamics. Automatica **48**(7), 1432–1439 (2012). https://doi.org/10.1016/j.automatica.2012.05.008
43. Khoo, S., Xie, L., Man, Z.: Robust finite-time consensus tracking algorithm for multi-robot systems. IEEE/ASME Trans. Mechatron. **14**(2), 219–228 (2009). https://doi.org/10.1109/TMECH.2009.2014057
44. Xiao, B., Yin, S., Gao, H.: Reconfigurable tolerant control of uncertain mechanical systems with actuator faults: A sliding mode observer-based approach. IEEE Trans. Control Syst. Technol. **26**(4), 1249–1258 (2017). https://doi.org/10.1109/TCST.2017.2707333
45. Ashraf, M.A., Ijaz, S., Zou, Y., Hamayun, M.T.: An integral sliding mode fault tolerant control for a class of non-linear Lipschitz systems. IET Control Theory & Applications **15**(3), 390–403 (2021). https://doi.org/10.1049/cth2.12050

Mahmoud Hussein received his B.S. and M.S. degrees in control systems from the Electrical Engineering Department, Sirte University, Sirte, Libya, and the University of Denver, Colorado, U.S.A., in 2004 and 2011, respectively, and the Ph.D. degree from the Electrical Engineering Department, École de technologie superieure (ÉTS), Univertsité du Québec, Montreal, Canada, in 2023. His current research interests include nonlinear control of mechanical systems, robotic systems, and fault-tolerant control design for networked control systems.

Youmin Zhang received his B.S., M.S., and Ph.D. degrees in automatic control from the Department of Automatic Control, Northwestern Polytechnical University, Xi'an, China, in 1983, 1986, and 1995, respectively. He is currently a Professor at the Department of Mechanical, Industrial and Aerospace Engineering, Concordia University, Canada. His research interests are in the areas of monitoring, diagnosis and physical fault/cyber-attack tolerant/resilient control, guidance, navigation and control of unmanned systems and smart grids, with applications to forest fires and smart cities in the framework of cyber-physical systems (CPSs) by combining with remote sensing techniques. He has published 10 books, over 600 journal and conference papers with high citations.

Dr. Zhang is a registered Professional Engineer in Ontario, Canada, a Fellow of IEEE (Institute of Electrical and Electronics Engineers) and CSME (Canadian Society of Mechanical Engineering), and a Member of Technical Committee for several scientific societies. He has been an Editor-in-Chief, Editorial Advisory Board Member of several journals, including as an Executive Advisory Board Member for "Journal of Intelligent & Robotic Systems", Associate Editor for "IEEE Transactions on Industrial Electronics", "IEEE Transactions on Neural Networks and Learning Systems", "IET Cyber-systems and Robotics", "Drone Systems and Applications", "Unmanned Systems", "Security and Safety", and Deputy EIC for "Guidance, Navigation and Control" etc. He has served as (Honorary) General Chair, Program Chair of several autonomous /unmanned systems, robotics and automation, renewable energies, smart cities relevant international conferences.

Zhaoheng Liu received his Ph.D. in Mechanical Engineering from the University of Sherbrooke, Canada in 1995. He was a postdoctoral research fellow at the University of Waterloo, Canada in 1996. He worked for six years as a research and development engineer at CM Labs Simulations Inc. and Maya HTT. In 2002, he joined École de technologie superieure (ÉTS), Univertsité du Québec, in the Department of Mechanical Engineering where he is currently a full professor. His research interests include vehicle dynamics, vibration of mechanical systems, robotic machining and nonlinear dynamics.